Anharmonic ground state selection in the pyrochlore antiferromagnet

U. Hizi* and C. L. Henley†
Laboratory of Atomic and Solid State Physics, Cornell University, Ithaca, New York 14853-2501, USA
(Received 23 January 2009; revised manuscript received 31 May 2009; published 7 July 2009)

In the pyrochlore lattice Heisenberg antiferromagnet, for large spin length S, the massive classical ground state degeneracy is partly lifted by the zero-point energy of quantum fluctuations at harmonic order in spin waves. However, there remains an infinite manifold of degenerate collinear ground states, related by a gaugelike symmetry. We have extended the spin-wave calculation to quartic order, assuming a Gaussian variational wave function (equivalent to Hartree-Fock approximation). Quartic calculations *do* break the harmonic-order degeneracy of periodic ground states. The form of the effective Hamiltonian describing this splitting, which depends on loops, was fitted numerically and also rationalized analytically. We find a family of states that are still almost degenerate, being split by the term from loops of length 26. We also calculated the anharmonic terms for the checkerboard lattice, and discuss why it (as well as the kagomé lattice) behave differently than the pyrochlore at anharmonic orders.

DOI: 10.1103/PhysRevB.80.014407 PACS number(s): 75.25.+z, 75.10.Jm, 75.30.Ds, 75.50.Ee

I. INTRODUCTION

Highly frustrated magnetic systems are systems in which there is a zero-temperature macroscopic classical ground state degeneracy.[1,2] In experimental systems, this degeneracy is generically broken by secondary interactions, or by lattice distortions.[3–5] However, even in toy models that include no such perturbations, one finds that the classical ground state degeneracy is broken by thermal fluctuations or quantum zero-point fluctuations. Such phenomena are collectively referred to as *order by disorder*.[6,7]

Among three-dimensional geometrically frustrated systems, the most studied, by far, is the pyrochlore lattice, which is composed of the centers of the bonds of a diamond lattice, so the pyrochlore sites form corner sharing tetrahedra. Despite numerous studies designed to illuminate on the ground state properties of this model, in the large-S limit,[3,4,8–13] a unique ground state has not been found for the pure undistorted pyrochlore Heisenberg model. In this paper, we answer this question by finding the effective Hamiltonian that represents the quantum zero-point energy to *anharmonic* order in spin waves. (A short report has appeared in Ref. 14).

We consider the nearest-neighbor Heisenberg Hamiltonian on the pyrochlore lattice

$$\mathcal{H} = J\sum_{\langle ij\rangle} \mathbf{S}_i \cdot \mathbf{S}_j. \tag{1.1}$$

Here and below, $\langle ij\rangle$ denotes a sum over nearest neighbors. Classically, all states satisfying

$$\sum_{i\in\alpha} \mathbf{S}_i = 0, \tag{1.2}$$

for all tetrahedra α are degenerate ground states, with energy $-JN_sS^2$, where N_s is the number of spins (we reserve Greek indices for tetrahedra (diamond-lattice sites) and roman indices for pyrochlore sites).

A. Prior work

In recent work,[9,11] we have studied the quantum zero-point fluctuations of the large-S limit of this model, and found that, to harmonic order in the $1/S$ expansion, there remains an infinite degeneracy of *collinear* spin states (although the entropy of this family is nonextensive). The degeneracy is associated with an exact invariance of the harmonic-order energy to a gaugelike transformation. Collinear configurations that are related by this symmetry have identical *fluxes* through all diamond-lattice loops, where the flux $\varphi_{\mathcal{L}}$ through loop $\mathcal{L}$ with bond centers at $(i_1, i_2, \ldots, i_{2n})$ is defined as

$$\varphi_{\mathcal{L}} = \eta_{i_1}\eta_{i_2}\eta_{i_3}\cdots\eta_{i_{2n}}. \tag{1.3}$$

The Ising variables $\eta_i = \pm 1$ correspond to the classical spin direction along the collinearity axis. The *harmonic ground states* are all of the Ising configurations in one of these *gauge families* and we call them the *π-flux states*, following Ref. 12. These consist of all collinear configurations whose fluxes through all *hexagons* (the shortest diamond-lattice loops) are negative,

$$\prod_{i\in\hexagon} \eta_i = -1, \quad \forall\, \hexagon. \tag{1.4}$$

[The argument for Eq. (1.4) is given in Sec. VI.] Some of these states are shown in Fig. 9 of Ref. 11. Furthermore, in Ref. 11, we constructed an effective Hamiltonian for the harmonic-order zero-point energy, of the form

$$E^{\text{eff}}_{\text{harm}} = N_sS(E_0 + K_6\Phi_6 + K_8\Phi_8 + \cdots), \tag{1.5}$$

where E_0 and K_n are numerical coefficients that can be evaluated analytically[11] ($E_0=-0.5640$, $K_6=0.0136$, $K_8=-0.0033$); here Φ_{2n} is the total flux (per lattice site) through all diamond-lattice loops of length $2n$,

$$\Phi_{2n} \equiv \frac{1}{N_s}\sum_{|\mathcal{L}|=2n} \varphi_{\mathcal{L}}. \tag{1.6}$$

In the interest of conciseness, throughout the rest of this paper we use the term *state* to mean "classical Ising configuration." In this paper, we go beyond the harmonic order in the expansion $1/S$, to search for a unique semiclassical ground state, focusing in the asymptotic $S\to\infty$ properties.

We consider small quantum fluctuations about classical Ising configurations such that the local collinear order is preserved. Our approach is aimed at deriving an *effective Hamiltonian*[15] in terms of a much small number of degrees of freedom.

Similar work has been previously done on the closely related kagomé lattice. This is a two-dimensional lattice, which is composed of corner sharing triangles. In the kagomé Heisenberg antiferromagnet the zero-temperature classical ground states satisfy Eq. (1.2) for all *triangles* α, and harmonic-order spin-wave fluctuations select *all* coplanar classical configurations as degenerate ground states. A self-consistent anharmonic theory breaks this degeneracy and selects one unique coplanar ground state—the so-called $\sqrt{3}\times\sqrt{3}$ state.[16–18]

B. Outline of the paper

This paper is organized as follows: in Sec. II we derive the large-S expansion by means of a Holstein-Primakoff transformation. We review some of the results of Ref. 11 on the harmonic theory. In Sec. III, we derive the mean-field Hamiltonian for the anharmonic theory, and present a self-consistent variational scheme for solving it.

Then, in Sec. IV we use a simple tractable example—the (π,π) state on the two-dimensional checkerboard lattice—in order to gain some analytic intuition on the behavior of the two-point correlation functions that governs the mean-field quartic energy, and the scaling laws involved. We find that these diverge as $\ln S$, resulting in anharmonic energy of order $(\ln S)^2$. In Sec. IV B we argue that among all of the checkerboard-lattice harmonic ground states, the quartic energy is minimized in the (π,π) state, and show numerical results to support this claim. We find that, due to the different symmetries of the checkerboard lattice and the Hamiltonian, the harmonic degeneracy in the checkerboard can be broken at the single-tetrahedron level, a result that cannot be carried over to the pyrochlore case.

In Sec. V we present the main results of this paper—numerical calculations for the pyrochlore lattice. We find that, as in the checkerboard, the quartic energy scales as $(\ln S)^2$. We calculate the anharmonic energy for a large set of harmonic ground states and find that and that the anharmonic theory breaks the degeneracy between them. We derive effective Hamiltonians for both the gauge-invariant and gauge-dependent terms in the quartic energy, and find a set of seemingly degenerate ground states.

Next, in Sec. VI, we present a real-space loop expansion to explain the nature of the dominant term in the gauge-dependent effective Hamiltonian. We analytically derive an effective Hamiltonian, which is different from the one we conjectured in the numerical fitting. Nevertheless the leading order terms of both effective Hamiltonians are minimized by the same set of states which, as far as we can tell, are all degenerate (both numerically and also to very high order in the effective Hamiltonian).

II. SPIN-WAVE THEORY

In this section, we expand the Hamiltonian (1.1) in the semiclassical limit, in powers of $1/S$. In Sec. II B we review some of the result in the harmonic theory of Ref. 11, relevant to this paper.

A. Large-S expansion

To study the quantum Heisenberg model, in the semiclassical limit of large S, we perform the Holstein-Primakoff transformation. Since the harmonic ground states are all collinear,[11] we shall, in the following, limit ourselves to states in which each site is labeled by an Ising variable η_i, such that, without loss of generality, the classical spin is $\mathbf{S}_i = \eta_i \hat{z}$ and $\Sigma_{i\in\alpha}\,\eta_i = 0$ for any tetrahedron α. Thus each tetrahedron includes four satisfied—antiferromagnetic (AFM)—bonds and two unsatisfied—ferromagnetic (FM)—bonds. Notice that, whenever the spins satisfy the classical ground state condition (1.2), the sum of neighbor spins is (-2) times the spin on a site, i.e.,

$$\sum_{j\text{n.n. of } i} \eta_j = -2\eta_i. \tag{2.1}$$

We first rotate the local coordinates to $(\eta_i\hat{x},\hat{y},\eta_i\hat{z})$ and define boson operators a_i and $a_i^\dagger$ such that

$$S_i^z = \eta_i(S - a_i^\dagger a_i),$$

$$S_i^+ \equiv \eta_i S^x + iS^y = \sqrt{2S - a_i^\dagger a_i}\,a_i,$$

$$S_i^- \equiv \eta_i S^x - iS^y = a_i^\dagger\sqrt{2S - a_i^\dagger a_i}. \tag{2.2}$$

These operators satisfy the canonic bosonic commutation relations

$$[a_i, a_j^\dagger] = \delta_{ij}, \quad [a_i, a_j] = 0, \quad [a_i^\dagger, a_j^\dagger] = 0. \tag{2.3}$$

We now expand Eq. (2.2) in powers of $1/S$, and express the Hamiltonian in terms of spin deviation operators

$$\sigma_i^x = \eta_i\sqrt{\frac{S}{2}}(a_i + a_i^\dagger), \quad \sigma_i^y = -i\sqrt{\frac{S}{2}}(a_i - a_i^\dagger), \tag{2.4}$$

and obtain[23]

$$\mathcal{H} = E_{\rm cl} + \mathcal{H}_{\rm harm} + \mathcal{H}_{\rm quart} + O(S^{-1}), \tag{2.5a}$$

$$E_{\rm cl} = -JN_sS^2, \tag{2.5b}$$

$$\mathcal{H}_{\rm harm} = \tilde{J}\sum_i[(\sigma_i^x)^2 + (\sigma_i^y)^2] + \tilde{J}\sum_{\langle ij\rangle}(\sigma_i^x\sigma_j^x + \sigma_i^y\sigma_j^y) - \tilde{J}SN_s, \tag{2.5c}$$

$$\begin{aligned}\mathcal{H}_{\rm quart} = \frac{\tilde{J}}{8S^2}\sum_{\langle ij\rangle}[&2\eta_i\eta_j((\sigma_i^x)^2 + (\sigma_i^y)^2)((\sigma_j^x)^2 + (\sigma_j^y)^2)\\ &- \sigma_i^x((\sigma_j^x)^3 + \sigma_j^y\sigma_j^x\sigma_j^y) - \sigma_j^x((\sigma_i^x)^3 + \sigma_i^y\sigma_i^x\sigma_i^y)\\ &- \sigma_i^y((\sigma_j^y)^3 + \sigma_j^x\sigma_j^y\sigma_j^x) - \sigma_j^y((\sigma_i^y)^3 + \sigma_i^x\sigma_i^y\sigma_i^x)].\end{aligned} \tag{2.5d}$$

where $\tilde{J}\equiv J(1+1/2S)$. In the following, we shall set $\tilde{J}=1$. Somewhat redundantly, we also define $\tilde{J}_{ij}\equiv\tilde{J}=1$ when (i,j)

are nearest neighbors, and zero otherwise (to simplify sums over just one index.)

B. Harmonic Hamiltonian

The use of the operators σ^x and σ^y allows us to represent the harmonic Hamiltonian (2.5c) in block diagonal form

$$\mathcal{H}_{\text{harm}} = \left((\boldsymbol{\sigma}^x)^\dagger, (\boldsymbol{\sigma}^y)^\dagger\right)\begin{pmatrix}\mathbf{H} & 0\\ 0 & \mathbf{H}\end{pmatrix}\begin{pmatrix}\boldsymbol{\sigma}^x\\ \boldsymbol{\sigma}^y\end{pmatrix} - \text{Tr}\mathbf{H}, \quad (2.6)$$

where $\boldsymbol{\sigma}^x$ and $\boldsymbol{\sigma}^y$ are vector operators with respect to site indices, of length N_s, and the $N_s \times N_s$ matrix $\mathbf{H}$ has elements

$$H_{ij} = \begin{cases} 1, & \text{if } i = j \\ \frac{1}{2}, & \text{if } i,j \text{ nearest neighbors} \\ 0, & \text{otherwise} \end{cases}. \quad (2.7)$$

The dependence on the particular classical ground state comes via the commutation relations

$$[\sigma_i^x, \sigma_j^y] = iS\eta_i\delta_{ij}. \quad (2.8)$$

in Ref. 11 we detailed the harmonic theory and the properties of the eigenmodes. Here we briefly summarize the results relevant to this paper, for completeness.

1. Diagonalization

Define the $N_s \times N_s$ diagonal matrix $\boldsymbol{\eta}$ by $\eta_{ij} \equiv \eta_i\delta_{ij}$. Then spin-wave modes of any Hamiltonian of form (2.6), with operator commutation relations (2.8) are the eigenvectors $\{\mathbf{v}_m\}$, with eigenvalues $\{\lambda_m\}$, of the *dynamical matrix* $\boldsymbol{\eta}\mathbf{H}$,

$$\eta_i\lambda_m v_m(i) = v_m(i) + \frac{1}{2}\sum_j \tilde{J}_{ij}v_m(j). \quad (2.9)$$

The eigenvectors satisfy a pseudo-orthogonality constraint

$$\mathbf{v}_l^\dagger \boldsymbol{\eta}\mathbf{v}_m \propto \delta_{lm}. \quad (2.10)$$

The corresponding frequencies are $\hbar\omega_m = 2S|\lambda_m|$, and thus the zero-point energy is

$$E_{\text{harm}} = S\sum_m (|\lambda_m| - 1). \quad (2.11)$$

In Refs. 9 and 11, it was shown that the zero-point energy is minimized for configurations that satisfy Eq. (1.4). A condensed version of this derivation shall be given later, in Sec. VI A.

For the Heisenberg Hamiltonian matrix on the pyrochlore lattice [Eq. (2.7)], one finds that (for *any* Ising ground state) half the spin-wave modes have vanishing frequencies. These are the *zero modes*, which satisfy

$$\sum_{i\in\alpha} v_m(i) = 0. \quad (2.12)$$

for all tetrahedra α. The two-point correlations (fluctuations) G_{ij} of the spin deviation operators, it can be shown, are given by

$$\mathbf{G} \equiv \langle \boldsymbol{\sigma}^x(\boldsymbol{\sigma}^x)^\dagger\rangle = \langle \boldsymbol{\sigma}^y(\boldsymbol{\sigma}^y)^\dagger\rangle = \sum_m \frac{S}{2}\frac{\mathbf{v}_m\mathbf{v}_m^\dagger}{|\mathbf{v}_m^\dagger\boldsymbol{\eta}\mathbf{v}_m|},$$

$$\langle \boldsymbol{\sigma}^x(\boldsymbol{\sigma}^y)^\dagger + \boldsymbol{\sigma}^y(\boldsymbol{\sigma}^x)^\dagger\rangle = \mathbf{0}. \quad (2.13)$$

It is clear from Eq. (2.13) that any mode $\mathbf{v}_m$ for which $\mathbf{v}_m^\dagger\boldsymbol{\eta}\mathbf{v}_m = 0$, exhibits divergent fluctuations. We call such a mode a *divergent mode* and it turns out that such a mode is necessarily a zero mode, i.e., $\lambda_m = 0$. The converse is not true–most zero modes have nonsingular fluctuations.

2. Ordinary modes

The eigenmodes of Eq. (2.9) can be divided into two groups: half $(N_s/2)$ of the modes have zero frequency. We call these *generic zero modes*[11] because the subspace that they span is identical for any collinear classical ground state.[19] Since these modes have zero frequency, they do not contribute to the harmonic zero-point energy.

The other half of the modes are called *ordinary modes*,[11] and these modes can be naturally expressed in terms of *diamond-lattice* modes (recall that the diamond lattice has $N_s/2$ sites): an (un-normalized) ordinary mode $\mathbf{v}_m$ can be written down as

$$v_m(i) = \frac{1}{\sqrt{2}}\eta_i \sum_{\alpha: i\in\alpha} u_m(\alpha), \quad (2.14)$$

where the sum runs over the two tetrahedra to which site i belongs and $\mathbf{u}_m$ is a vector of length $N_s/2$, living on the centers of tetrahedra (diamond-lattice sites), and satisfying the spin-wave equation

$$\lambda_m u_m(\alpha) = \frac{1}{2}{\sum_\beta}' \eta_{i(\alpha\beta)}u_m(\beta), \quad (2.15)$$

where the sum is over (diamond-lattice) nearest neighbors of α, and $i(\alpha\beta)$ is the pyrochlore site on the center of the bond connecting α and β. The diamond-lattice modes $\{\mathbf{u}_m\}$ are eigenmodes of an Hermitian matrix and therefore are orthogonal to each other in the usual sense. We choose the normalization $|\mathbf{u}_m| = 1$ without loss of generality. From Eqs. (2.14) and (2.15) one easily simplifies the pseudonorm denominator in Eq. (2.13),

$$\mathbf{v}_m^\dagger\boldsymbol{\eta}\mathbf{v}_m = \lambda_m \quad (2.16)$$

(valid only for ordinary modes).

It is evident that the solutions of Eq. (2.15) are invariant under a *gaugelike transformation* of the state: if we transform $\eta_i \to \tau_\alpha\tau_\beta\eta_i$, where $\tau_\alpha, \tau_\beta = \pm 1$, then the dispersion would not change, and the ordinary modes would transform $u_m(\alpha) \to \tau_\alpha u_m(\alpha)$. Taking $\tau_\alpha = -1$ amount to flipping all of the spins in tetrahedron α. Such a transformation is not literally a gauge transformation since the flips must be correlated so that the tetrahedron rule—$\Sigma_{i\in\alpha}\ \eta_i = 0$ from (1.2)—is preserved. Whenever two states are related by a gaugelike transformation, they have the same spin-wave eigenvalues λ_m and hence identical values of the total harmonic zero-point energy.

Although most of the ordinary modes carry nonzero frequency, there is a subset of them that has $\lambda_m = 0$. It turns out

that these are the divergent modes–modes that have $\mathbf{v}_m^\dagger \boldsymbol{\eta} \mathbf{v}_m = 0$, and whose correlations are divergent [see Eqs. (2.13) and (2.16)].

3. Fourier-transformed Hamiltonian

In order to perform numerical calculations on large systems, we must limit ourselves to periodic states. We shall assume a *magnetic unit cell* with N_M sites arranged on a *magnetic lattice*. In the simplest possible $\mathbf{Q}=0$ case, $N_M=4$ and the magnetic lattice is the fcc. Most of this work focuses on harmonic ground states, i.e., π-flux states. The *smallest* possible unit cell for that case has $N_M=16$ sites. In practice, the calculation can often be simplified by utilizing the *bond order*, which may have a smaller unit cell.[20]

We Fourier transform Hamiltonian (2.6),

$$\mathcal{H}_{\text{harm}} = \sum_{\mathbf{q}} [(\boldsymbol{\sigma}_{\mathbf{q}}^x)^\dagger, (\boldsymbol{\sigma}_{\mathbf{q}}^y)^\dagger] \begin{pmatrix} \mathbf{H}(\mathbf{q}) & \mathbf{0} \\ \mathbf{0} & \mathbf{H}(\mathbf{q}) \end{pmatrix} \begin{pmatrix} \boldsymbol{\sigma}_{-\mathbf{q}}^x \\ \boldsymbol{\sigma}_{-\mathbf{q}}^x \end{pmatrix} - \mathrm{Tr}\mathbf{H}(\mathbf{q}), \tag{2.17}$$

where $\boldsymbol{\sigma}_{\mathbf{q}}^x$ and $\boldsymbol{\sigma}_{\mathbf{q}}^y$ are vectors of length N_M of the Fourier-transformed x and y spin deviation operators. The wave vector $\mathbf{q}$ is in the Brillouin zone of the magnetic lattice,

$$\vec{\sigma}_i = \frac{1}{\sqrt{N_M}} \sum_{\mathbf{q}} \vec{\sigma}_{\mathbf{q}}^{l_i} e^{-i\mathbf{q}\cdot[\mathbf{R}_i + \boldsymbol{\Delta}_{l_i}]},$$

$$\vec{\sigma}_{\mathbf{q}}^l = \frac{1}{\sqrt{N_M}} \sum_{\mathbf{R}} \vec{\sigma}_{\mathbf{R}}^l e^{i\mathbf{q}\cdot(\mathbf{R}+\boldsymbol{\Delta}_l)}, \tag{2.18}$$

where $\mathbf{R}$ is a magnetic lattice vector and l is a sublattice index, corresponding to a basis vector $\boldsymbol{\Delta}_l$, i.e., for site i: $\mathbf{r}_i = \mathbf{R}_i + \boldsymbol{\Delta}_{l_i}$

Upon diagonalization of the Hamiltonian [i.e., finding eigenmodes of $\boldsymbol{\eta} H(\mathbf{q})$, where $\boldsymbol{\eta}$ is now $N_M \times N_M$], we obtain N_M bands within the Brillouin zone, half of which are of zero mode bands, and half are of ordinary modes. The divergent spin-wave modes can be shown to occur along *lines* in the Brillouin zone where an ordinary-mode frequency goes to zero (we call these *divergence lines*).[11] Each of these divergence lines is parallel to one of x, y, or z axes.

The correlations of spin fluctuations can be expanded in terms of Fourier components, using Eq. (2.18),

$$G_{ij} \equiv \langle \sigma_i \sigma_j \rangle \frac{N_M}{N_s} \sum_{\mathbf{q}} G_{l_i l_j}(\mathbf{q}) \cos \boldsymbol{\chi}_{ij} \cdot \mathbf{q}, \tag{2.19}$$

with

$$G_{l_i l_j}(\mathbf{q}) \equiv \langle \sigma_{\mathbf{q}}(l_i) \sigma_{-\mathbf{q}}(l_j) \rangle, \tag{2.20}$$

where l_i and l_j are the sublattice indices of i and j, respectively, and $\boldsymbol{\chi}_{ij} = \mathbf{r}_i - \mathbf{r}_j$.

III. SELF-CONSISTENT ANHARMONIC THEORY

This section develops our mean-field prescription to self-consistently calculate the anharmonic corrections to the energy, for an arbitrary given state $\{\eta_i\}$. First, (Sec. III A 1) we decouple the quartic term $\mathcal{H}_{\text{quart}}$ and write down a quadratic mean-field Hamiltonian. Next, we introduce a variational Hamiltonian as an approximation for mean-field problem (Sec. III B), and in Sec. III B 3 show that the variational form agrees with a general self-consistent approach in the large-S limit. In Sec. III C we discuss how various fluctuations and energy scales depend on S.

A. Decoupling scheme

First let us work through the Hartree-Fock-like decoupling of the quartic term (2.5d) of our spin-wave Hamiltonian.[20] It turns out the decoupled coefficients depend on the (Ising) spin configuration in a simple fashion (Sec. III A 2) which allows us (in principle) to reduce the self-consistency conditions to a one-parameter equation.

1. Energy expectation and decoupled Hamiltonian

In a decoupling, one implicitly assumes a variational wave function Ψ_{MF}, *a priori* unconstrained except for being Gaussian. Thus, it is specified by a harmonic effective Hamiltonian $\mathcal{H}_{\text{MF}}$, defined so that

$$\langle \mathcal{H}_{\text{harm}} + \mathcal{H}_{\text{quart}} \rangle = \langle \mathcal{H}_{\text{MF}} \rangle, \tag{3.1}$$

where the expectations are taken with respect to $\mathcal{H}_{\text{MF}}$ itself.

In light of Wick's theorem, we can immediately write the energy expectation by plugging into Eqs. (2.5c) and (2.5d) the two-point correlations defined in Eq. (2.13), but now using the $\mathcal{H}_{\text{MF}}$ wave function,

$$\langle \mathcal{H}_{\text{harm}} \rangle = 2\left(\sum_i G_{ii} + \sum_{\langle ij \rangle} G_{ij} - SN_s \right), \tag{3.2a}$$

$$\langle \mathcal{H}_{\text{quart}} \rangle = \frac{1}{2S^2} \sum_{\langle ij \rangle} [\eta_i \eta_j (G_{ii} G_{jj} + G_{ij}^2) - G_{ij}(G_{ii} + G_{jj})]. \tag{3.2b}$$

To make some expressions more compact, we define a bond variable,

$$\Gamma_{ij} \equiv G_{ii} - \eta_i \eta_j G_{ij}. \tag{3.3}$$

Γ_{ij} is, in general, *not* symmetric[21] and is defined only for (i,j) nearest neighbors (nonzero $\tilde{J}_{ij}$).

Substituting Eq. (3.3) into Eq. (3.2), and using Eq. (2.1), we get

$$\langle \mathcal{H}_{\text{harm}} \rangle = -\sum_{\langle ij \rangle} [\eta_i \eta_j (\Gamma_{ij} + \Gamma_{ji}) - SN_s], \tag{3.4a}$$

$$\langle \mathcal{H}_{\text{quart}} \rangle = \frac{1}{S^2} \sum_{\langle ij \rangle} \eta_i \eta_j \Gamma_{ij} \Gamma_{ji}. \tag{3.4b}$$

Then

$$E_{\mathrm{MF}} \equiv \langle \mathcal{H}_{\mathrm{MF}} \rangle = -\sum_{ij} (H_{\mathrm{MF}})_{ij} G_{ij} = -\sum_{\langle ij \rangle} \eta_i \eta_j \left(\Gamma_{ij} + \Gamma_{ji} - \frac{1}{S^2} \Gamma_{ij} \Gamma_{ji} \right) - SN_s, \tag{3.5}$$

and [using Eq. (3.2)] we see indeed that $\mathcal{H}_{\mathrm{MF}}$ satisfies Eq. (3.1).

To write our decoupled Hamiltonian $\mathcal{H}_{\mathrm{quart}}+\mathcal{H}_{\mathrm{harm}}$, we adopt a matrix form, in analogy with the harmonic Hamiltonian (2.6),

$$\mathcal{H}_{\mathrm{MF}} = [(\boldsymbol{\sigma}^x)^\dagger, (\boldsymbol{\sigma}^y)^\dagger] \begin{pmatrix} \mathbf{H}_{\mathrm{MF}} & \mathbf{0} \\ \mathbf{0} & \mathbf{H}_{\mathrm{MF}} \end{pmatrix} \begin{pmatrix} \boldsymbol{\sigma}^x \\ \boldsymbol{\sigma}^y \end{pmatrix} - SN_s, \tag{3.6}$$

defining the matrix elements in Eq. (3.6) to depend on the correlations G_{ij},

$$(H_{\mathrm{MF}})_{ij} = \frac{\tilde{J}_{ij}}{2} \left[1 - \frac{G_{ii} + G_{jj} - 2\eta_i \eta_j G_{ij}}{2S^2} \right], \tag{3.7a}$$

$$(H_{\mathrm{MF}})_{ii} = 1 + \frac{1}{2S^2} \sum_j \tilde{J}_{ij} (\eta_i \eta_j G_{jj} - G_{ij}). \tag{3.7b}$$

Recall from Sec. II A that $\tilde{J}_{ij}=1$ for nearest neighbors, otherwise zero. Thus, although G_{ij} decays as a power law, $\mathcal{H}_{\mathrm{MF}}$ has only on-site and nearest-neighbor terms. In terms of the Γ_{ij} variables, Eq. (3.7) reads

$$(H_{\mathrm{MF}})_{ij} = \frac{\tilde{J}_{ij}}{2} \left[1 - \frac{1}{2S^2} (\Gamma_{ij} + \Gamma_{ji}) \right], \tag{3.8a}$$

$$(H_{\mathrm{MF}})_{ii} = 1 + \frac{1}{2S^2} \sum_j \tilde{J}_{ij} \eta_i \eta_j \Gamma_{ji}. \tag{3.8b}$$

All the machinery that was applied to $\mathbf{H}$ for the harmonic problem in Sec. II B can now be applied to $\mathbf{H}_{\mathrm{MF}}$. In particular, we can evaluate the correlations $\{G_{ij}\}$, in terms of which the Hamiltonian matrix elements are written. Thus, by the self-consistent decoupling approximation we have replaced the interacting spin-wave Hamiltonian by an effective noninteracting theory.

Unfortunately, this does not yet give a solution since the $\{G_{ij}\}$ are *a priori* unknown. We cannot just use the correlations obtained from the bare harmonic theory (2.6) for both practical reasons (G_{ij} diverges in that case) and substantive ones: the theory would not be self-consistent—we would not recover the same correlations as those we put into it. A solution may in fact be obtained by successive iterations: assume a trial set of coefficients $\mathbf{H}_{\mathrm{MF}}$, compute the implied correlations, and define the next iteration of $\mathbf{H}_{\mathrm{MF}}$ from Eq. (3.7a).

2. Simplified form of Γ_{ij} and $\mathcal{H}_{\mathrm{MF}}$

In principle this iteration seems forbidding, but it is simplified by an important fact, discovered numerically but verified analytically. For any $\mathcal{H}_{\mathrm{MF}}$ approaching $\mathcal{H}_{\mathrm{harm}}$, as should be the case for large S,

$$\Gamma_{ij} = \Gamma^{(0)} + \Gamma^{(2)} \eta_i \eta_j + \Delta\Gamma_{ij}. \tag{3.9}$$

Here $\Gamma^{(0)}$ and $\Gamma^{(2)}$ are diverging terms independent of i, j (and of the same order), whereas $\Delta\Gamma_{ij}$ does depend on i and j, but is much smaller than $\Gamma^{(2)}$. This was seen numerically in the outputs from a particular family of starting parameters, the family of variational wave functions $\Psi(\varepsilon)$ specified by $\mathcal{H}_{\mathrm{var}}(\varepsilon)$ [defined below in Sec. III B]. More generally, an analytic explanation of form (3.9), i.e., why Γ_{ij} depends only on $\eta_i \eta_j$ at dominant order, is found in Appendix A. [It follows from the gaugelike invariance, for the special case of Ising configurations that minimize the harmonic energy, the π-flux states]. One might crudely paraphrase that argument by saying the correlations that come out of the bare Hamiltonian have the form as Eq. (3.9) (albeit with divergent $\Gamma^{(0)}$, $\Gamma^{(2)}$).

Next, inserting relation (3.9) into Eqs. (3.8), we can write the matrix elements of the mean-field Hamiltonian

$$(H_{\mathrm{MF}})_{ij} = \frac{\tilde{J}_{ij}}{2} \left[\left(1 - \frac{1}{S^2} \Gamma^{(0)} \right) - \frac{1}{S^2} \Gamma^{(2)} \eta_i \eta_j - \frac{1}{2S^2} (\Delta\Gamma_{ij} + \Delta\Gamma_{ji}) \right], \tag{3.10a}$$

$$(H_{\mathrm{MF}})_{ii} = \left(1 - \frac{1}{S^2} \Gamma^{(0)} \right) + \frac{3}{S^2} \Gamma^{(2)} + \frac{1}{2S^2} \sum_j \tilde{J}_{ij} \eta_i \eta_j \Delta\Gamma_{ji}. \tag{3.10b}$$

To get the last line of Eq. (3.10b), we used the $z=6$ coordination of the pyrochlore lattice, and the classical tetrahedron constraint $\Sigma_{i \in \alpha}\ \eta_i = 0$ [from Eq. (1.2)]. We now define

$$J^* \equiv 1 - \frac{1}{S^2} \Gamma^{(0)}, \quad J^*_{ij} \equiv J^* \tilde{J}_{ij}. \tag{3.11}$$

Note that $|J^* - 1| \ll 1$. We obtain

$$(H_{\mathrm{MF}})_{ij} = \frac{J^*_{ij}}{2} (1 - \eta_i \eta_j) - \frac{1}{2S^2} (\Delta\Gamma_{ij} + \Delta\Gamma_{ji}), \tag{3.12a}$$

$$(H_{\mathrm{MF}})_{ii} = J^* \left(1 + \frac{3}{4} \varepsilon_{\mathrm{out}} \right) + \frac{1}{2S^2} \sum_j \tilde{J}_{ij} \eta_i \eta_j \Delta\Gamma_{ji}, \tag{3.12b}$$

where

$$\varepsilon_{\mathrm{out}} \equiv \frac{4\Gamma^{(2)}}{S^2 J^*}. \tag{3.13}$$

Thus, if we drop the much smaller terms in $\Delta\Gamma_{ij}$ all the corrections are proportional to a single parameter $\Gamma^{(2)}$ times simple functions of the spin configuration.

B. Variational hamiltonian

The one-parameter dependence of Eq. (3.12) suggests we do not need to explore the full parameter space of trial Hamiltonians to find the self-consistent mean-field Hamiltonian. Instead, we shall limit ourselves to a simplified varia-

tional Hamiltonian $\mathcal{H}_{\rm var}$, which though it has just one variational parameter, appears to capture all the important properties of $\mathcal{H}_{\rm MF}$. (Specifically, $\mathcal{H}_{\rm var}$ approximates $\mathcal{H}_{\rm MF}$ better and better in the limit $S\to\infty$, as will be shown analytically below.)

So, we wish to write a harmonic $\mathcal{H}_{\rm var}$, as simple as possible, to specify the Gaussian variational wave function $\Psi_{\rm var}$, its ground state (not necessarily equal to $\Psi_{\rm MF}$). Since $\mathcal{H}_{\rm MF}$—the solution to an unconstrained variational problem—has only nearest-neighbor terms, there is no loss of generality when we restrict our variational search to that form. [In contrast, on the kagomé lattice, the appropriate variational Hamiltonian had second- or third-nearest-neighbor (Heisenberg) terms,[16–18,22] due to cubic terms in the spin-wave expansion.] We thus adopt the simplest nontrivial form, the same as Eq. (3.6), except with the diagonal block matrix $\mathbf{H}_{\rm MF}$ replaced by

$$\mathbf{H}_{\rm var} \equiv \mathbf{H} + \delta\boldsymbol{\eta}\mathbf{H}\boldsymbol{\eta} + \varepsilon\mathbb{1}. \tag{3.14}$$

where δ and ε are variational parameters. The δ modifies the strength of AFM and FM bonds in opposite ways: namely, $(H_{\rm var})_{ij}=(1+\delta)/2$ for neighbors with $\eta_i=\eta_j$ and $(H_{\rm var})_{ij}=(1-\delta)/2$ for neighbors with $\eta_i=-\eta_j$. This is the simplest possible form of a variational Hamiltonian that is consistent with the local spin symmetries.

We do require invariance under global spin rotations, which means the Goldstone mode (associated with global rotation) must have zero energy. Its eigenvector $\mathbf{v}_G$ has elements

$$v_G(i) = \frac{\eta_i}{\sqrt{N_s}}, \quad \forall\, i. \tag{3.15}$$

Thus we require $\boldsymbol{\eta}\mathbf{H}_{\rm var}\mathbf{v}_G=0$; inserting Eq. (3.7b) and writing out each term, we first note $\mathbf{H}\mathbf{v}_G=0$ so our condition is

$$0 = \eta_i \sum_j (H_{\rm var})_{ij} v_G(j) = 4\delta + \varepsilon. \tag{3.16}$$

Thus Eq. (3.14) ends up having only one independent variational parameter ε. It will become clear in the following that the correct signs for the parameters are $\varepsilon>0$, $\delta<0$. So, just writing out the components of $\mathbf{H}_{\rm var}$ as defined in Eq. (3.14),

$$(H_{\rm var})_{ij} = \frac{1}{2}\left(1 - \frac{\varepsilon}{4}\eta_i\eta_j\right), \tag{3.17a}$$

$$(H_{\rm var})_{ii} = 1 + \frac{3}{4}\varepsilon. \tag{3.17b}$$

Note that (ij) in Eq. (3.17a), and in similar equation pairs, applies only to nearest-neighbor sites.

A more elaborate (multiparameter) trial form of $\mathcal{H}_{\rm var}$ might improve the quality of the calculation, by exploring a larger set of variational wave functions; this is particularly important when the Ising configuration is not uniform from the gauge-invariant viewpoint (see Appendix A 2) since Eq. (3.9) breaks down in that case. Nevertheless, as we shall see numerically in Sec. V, the most important degeneracy-breaking effects are captured within this simple one-parameter theory.

1. Self-consistent approach

Revisiting Eqs. (3.12), we see they reduce to Eqs. (3.17) but with $\varepsilon\to\varepsilon_{\rm out}$. Furthermore, as $\varepsilon\to 0$, it turns out $\varepsilon_{\rm out}(\varepsilon)$ is *increasing* [indeed logarithmically divergent: see Eqs. (4.17) and (5.1)]. So there is a unique self-consistent solution to

$$\varepsilon^*_{\rm SC} = \varepsilon_{\rm out}(\varepsilon^*_{\rm SC}) = \frac{4\Gamma^{(2)}(\varepsilon^*_{\rm SC})}{S^2 J^*}. \tag{3.18}$$

and at $\varepsilon=\varepsilon^*_{\rm SC}$, [neglecting the $\Delta\Gamma_{ij}$ correction terms] we get

$$\mathbf{H}_{\rm MF} \approx J^*\mathbf{H}_{\rm var}. \tag{3.19}$$

Of course, the overall prefactor of J^* has no effect on the spin correlations comprising Γ_{ij}. Thus we have shown that, up to small corrections (of $\Delta\Gamma_{ij}$), we in fact get out the same $\mathcal{H}_{\rm MF}$ that we put in so our theory is self-consistent. The only condition required for this to work was Eq. (3.9).

Note $\Gamma^{(0)}$ and $\Gamma^{(2)}$ are of order $S\ln\varepsilon$, as will be explicitly verified analytically for the checkerboard lattice (Sec. IV A 2) and the pyrochlore (Sec. V A). The correction $|\Delta\Gamma_{ij}|$ in Eq. (3.9) is an order of magnitude smaller than $\Gamma^{(2)}$ for all tractable values of ε.

If we had tried a different one-parameter form of variational Hamiltonian, where we add $\pm\delta$ to the matrix elements $\mathbf{H}_{ij}$ in a pattern other than the one in Eq. (3.14), the divergent Γ_{ij} would indeed be regularized, but the dominant contribution would still be of form (3.9) so self-consistency is lost: the output would not have the same as the input. The only one-parameter nearest-neighbor variational Hamiltonian which is self-consistent is Eq. (3.14).

2. Variational approach

The above recipe is perfectly valid, but our actual calculation was done somewhat differently. We diagonalized the $\mathcal{H}_{\rm var}$ to find a variational wave function $\Psi_{\rm var}(\varepsilon)$ and its correlations $\{G_{ij}\}$, and computed an expectation $E_{\rm MF}(\varepsilon,S)$ [given by Eq. (3.5)]. We iteratively minimized $E_{\rm MF}(\varepsilon,S)$ with respect to ε (for a given S), defining a unique optimal value $\varepsilon=\varepsilon^*(S)$.

It will be shown below (in Sec. IV A 2 and V A) that $\varepsilon^*(S)\propto \ln S/S$.

3. Equivalence of self-consistent and variational approaches

It remains to be justified that $\varepsilon^*_{\rm SC}$, defined self-consistently, should equal ε^*, defined by minimizing $E_{\rm MF}$. This is expected since the decoupling is variationally based: that is, a *full* variational optimization of $\mathcal{H}_{\rm MF}$ with respect to all its parameters is equivalent to self-consistency with the decoupling form, by construction. Thus, to the extent the full solution sticks within the subspace defined by $\mathcal{H}_{\rm var}$ (as we argued it did), the decoupling and variational minimization (both within that subspace) ought to agree with each other.

The test for whether our result really is self-consistent is that the diagonal elements of Eq. (3.7b) should be independent of i, and the off-diagonal elements of Eq. (3.7a) should depend solely on $\eta_i\eta_j$. Furthermore, we want $(H_{\rm MF})_{ij}/(H_{\rm var})_{ij}$ to be equal for all i, j (for which $H_{ij}\neq 0$). We indeed found

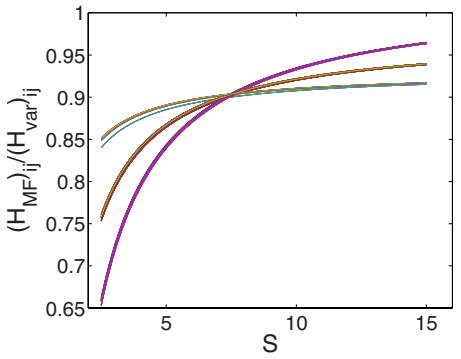

FIG. 1. (Color online) Self-consistency of the matrix elements. We show the ratio of all nonzero elements of $\mathbf{H}_{\mathrm{MF}}$ and $\mathbf{H}_{\mathrm{var}}(\varepsilon)$ for the state shown in Fig. 9(d) of Ref. 11. Here ε is set to 0.1. Each line represents a particular (ij) matrix element. Up to symmetries of the configuration, there are eleven unique matrix elements for this state, some of which are virtually indistinguishable in the plot. All of the lines converge at $S^*(\varepsilon=0.1)=7.5$ (up to a deviation which is much smaller than ε).

(empirically) that this works when $\varepsilon=\varepsilon^*(S)$, i.e., [letting $S^*(\varepsilon)$ be the inverse relation to $\varepsilon^*(S)$]

$$\mathrm{variance}_{ij}\left\{\frac{(H_{\mathrm{MF}}(S^*(\varepsilon)))_{ij}}{(H_{\mathrm{var}}(\varepsilon))_{ij}}\right\} \ll \varepsilon. \tag{3.20}$$

In Fig. 1 we show an example of this for a particular state and a particular value of ε. The crossing defines $\varepsilon^*{}_{\mathrm{SC}}$, in light of Eq. (3.19), but it is seen to happen exactly where $\varepsilon=\varepsilon^*$, thus empirically confirming the equivalence.

C. Scaling

Within the harmonic theory of Sec. II B, the fluctuations of the spin deviation operators scale as $\langle\sigma_i\sigma_j\rangle=\mathcal{O}(S)$—we omit the x and y component labels in these schematic expressions—and therefore we would naively expect, from the spin-wave expansion (2.5), that

$$E_{\mathrm{harm}}=\mathcal{O}(S), \quad \langle\mathcal{H}_{\mathrm{quart}}\rangle_{\mathrm{naive}}=\mathcal{O}(1). \tag{3.21}$$

However, $\mathcal{H}_{\mathrm{quart}}$ has an infinite expectation using the unmodified ground state wave function of $\mathcal{H}_{\mathrm{harm}}$ since the fluctuations diverge. Studies of the kagomé lattice[16–18] have taught us that when anharmonic terms are treated self-consistently, spin fluctuations of *divergent modes* are renormalized to finite values. In the kagomé case $\langle\sigma_i\sigma_j\rangle=\mathcal{O}(S^{4/3})$ and the scaling relations are

$$E_{\mathrm{harm}}=\mathcal{O}(S), \quad \langle\mathcal{H}_{\mathrm{quart}}\rangle_{\mathrm{kag}}=\mathcal{O}(S^{2/3}). \tag{3.22}$$

Note that the harmonic energy is not rescaled because the frequency of divergent zero modes is only $\mathcal{O}(S^{2/3})$, which is negligible compared to the frequency $[\mathcal{O}(S)]$ of modes other than zero modes.

One might expect scaling (3.22) to carry through to the pyrochlore lattice as well.[23] However, the divergent modes of the kagomé and the pyrochlore are rather different: in the kagomé, due to the anisotropy between in-plane and out-of-plane spin fluctuations, *all* zero modes are divergent modes so the kagomé divergent modes span the entire Brillouin zone. In the pyrochlore, on the other hand, the divergent modes reside only along lines in the Brillouin zone: hence the divergences (coming from these lines' vicinity) are weaker. Below [see Eqs. (4.17) and (5.1)] we shall find that this leads to *logarithmic* renormalization of the divergent fluctuations $\Gamma_{ij}=\mathcal{O}(S\ln S)$, resulting in scaling

$$\langle\mathcal{H}_{\mathrm{quart}}\rangle \equiv E_{\mathrm{MF}}-E_{\mathrm{harm}}=\mathcal{O}[(\ln S)^2]. \tag{3.23}$$

The singularity of the divergent modes' fluctuations, away from $\mathbf{q}=0$, is cut off by the variational parameter ε. At $\mathbf{q}=0$, the divergence of $\langle\sigma_i\sigma_j\rangle$ would be preserved, due to the physical Goldstone mode $\mathbf{v}_G$, but the Goldstone mode's contribution to Γ_{ij} vanishes such that the Goldstone mode does not contribute to the energy at any order in $1/S$.

Because it is technically difficult to deal with the divergence of $G_{ij}(\mathbf{q}=0)$ we shall, for now, retain both variational parameters. Thus we will have a handle on the fluctuations until we eventually take the limit $\delta\to-\varepsilon/4$. [We find that $G_{ij}(\mathbf{q}=0)\sim 1/\sqrt{\varepsilon+4\delta}$ so that $\varepsilon+4\delta$ must be chosen to be positive.]

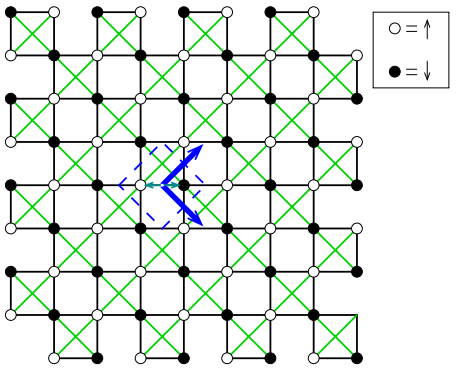

FIG. 2. (Color online) The checkerboard lattice (π,π) state. The primitive vectors are the diagonal arrows, and the primitive unit cell is shown by the dashed square. The small arrows represents the two basis vectors. Here we show the (π,π) state: open (closed) circles denote up (down) spins. Dark (light) colored lines denote AFM (FM) bonds.

IV. CHECKERBOARD LATTICE

As a warm up to the pyrochlore lattice problem, we first consider the same model on the closely related two-dimensional checkerboard lattice. This case is more tractable, in that some expressions have a simple form which could not (or should not) be written out analytically in the pyrochlore case.

The checkerboard lattice (see Fig. 2) can be viewed as {001} projection of the pyrochlore lattice, and is often called the *planar pyrochlore*. The lattice structure is a square lattice with primitive vectors (1,1) and (1,−1) and two sublattices corresponding to basis vectors (−1/2,0) and (1/2,0). We refer to the crossed squares as "tetrahedra" in analogy with the pyrochlore lattice, and we refer to any two sites within a tetrahedron as "nearest neighbors" regardless of the actual bond length.

Since the checkerboard lattice, as the pyrochlore, is composed of corner sharing tetrahedra, the derivation of Sec. II remains valid. Note that we assume that all of the couplings within a tetrahedron are equal, even though in the checkerboard lattice, the various bonds are not related by lattice symmetries. Since the shortest loop in the checkerboard lattice is a square, the effective harmonic Hamiltonian for this lattice has the same form as the pyrochlore lattice harmonic effective Hamiltonian (1.5), with the addition of a dominant term $K_4\Phi_4$, with $K_4<0$.[11,13]

Thus, the harmonic ground states of the checkerboard lattice consist of all the zero-flux states, i.e., states with positive flux in all square plaquettes. Similar to the pyrochlore case, this is a family of states that are exactly degenerate to harmonic order, and in this case the residual entropy is $\mathcal{O}(L)$, where L is the linear dimension of the system.[11] But since lattice does not respect the full symmetry of the tetrahedron, the selection effect of the anharmonic terms turns out quite different (and essentially trivial) as compared to the pyrochlore case.

A. Checkerboard (π,π) state

One of the checkerboard harmonic ground states is simple enough for the diagonalization of variational Hamiltonian (3.14) to be done analytically: the (π,π) state depicted in Fig. 2. In this state, the diagonal bonds in each tetrahedron are unsatisfied (FM) such that the symmetry of the lattice is conserved, and the magnetic unit cell has two sites.

1. Harmonic Hamiltonian for checkerboard

The Fourier-transformed harmonic Hamiltonian for the (π,π) state is Eq. (2.17), with

$$\mathbf{H}(\mathbf{q}) = \begin{pmatrix} 2\cos^2 Q_+ & 2\cos Q_+ \cos Q_- \\ 2\cos Q_+ \cos Q_- & 2\cos^2 Q_- \end{pmatrix}, \quad (4.1)$$

where

$$Q_\pm \equiv (q_x \pm q_y)/2. \quad (4.2)$$

The spin-wave modes can be found by diagonalizing the matrix $\boldsymbol{\eta}\mathbf{H}(\mathbf{q})$.[11] $\boldsymbol{\eta}$ is a diagonal matrix with elements $\{\eta_i\}$ along the diagonal (in our case $\eta_1=1$, $\eta_2=2$). Diagonalization of $\boldsymbol{\eta}\mathbf{H}(\mathbf{q})$ produces eigenmodes $\mathbf{V}_\mathbf{q}$ and $\mathbf{U}_\mathbf{q}$ for any wave vector $\mathbf{q}$,

$$\mathbf{V}_\mathbf{q}^T = \sqrt{\frac{2}{\alpha_\mathbf{q}}}(\cos Q_+, -\cos Q_-), \quad \lambda_V = \beta_\mathbf{q},$$

$$\mathbf{U}_\mathbf{q}^T = \sqrt{\frac{2}{\alpha_\mathbf{q}}}(\cos Q_-, -\cos Q_+), \quad \lambda_U = 0, \quad (4.3)$$

satisfying the pseudo-orthogonality condition $\mathbf{V}_\mathbf{q}^\dagger \boldsymbol{\eta}\mathbf{U}_\mathbf{q}=0$. The dispersions corresponding to $\mathbf{V}_\mathbf{q}$ and $\mathbf{U}_\mathbf{q}$, respectively, are

$$\lambda_{\mathbf{V}_\mathbf{q}} = \beta_\mathbf{q}, \quad \lambda_{\mathbf{U}_\mathbf{q}} = 0. \quad (4.4)$$

Here we defined

$$\alpha_\mathbf{q} = 2(\cos^2 Q_+ + \cos^2 Q_-),$$

$$\beta_\mathbf{q} = 2(\cos^2 Q_+ - \cos^2 Q_-). \quad (4.5)$$

Thus, the ordinary spin-wave band has dispersion $\hbar\omega_\mathbf{q} = 2S|\beta_\mathbf{q}|$, and the zero-point energy can be easily calculated,

$$E_{\text{harm}} = \frac{1}{2}\sum_\mathbf{q} \hbar\omega_\mathbf{q} - N_s S = N_s S\left(\frac{4}{\pi^2} - 1\right). \quad (4.6)$$

The fluctuations of the spin deviation operators $[G_{lm}(\mathbf{q}) = \langle \sigma^x_\mathbf{q}(l)\sigma^x_{-\mathbf{q}}(m)\rangle$, where l and m are sublattice indices] can be calculated from the spin-wave modes by Eq. (2.13),

$$\mathbf{G}(\mathbf{q}) = \frac{S}{2\beta_\mathbf{q}}\begin{pmatrix} \alpha_\mathbf{q} & -\gamma_\mathbf{q} \\ -\gamma_\mathbf{q} & \alpha_\mathbf{q} \end{pmatrix}, \quad (4.7)$$

where $\gamma_\mathbf{q} \equiv 4\cos Q_+ \cos Q_-$ so that $\alpha_\mathbf{q} = \sqrt{\beta_\mathbf{q}^2 + \gamma_\mathbf{q}^2}$. Equation (4.7) shows that the fluctuations diverge wherever $\beta_\mathbf{q}$ vanishes, i.e., along the lines in the Brillouin zone $|Q_+| = |Q_-|$, which turn out to be $q_x=0$ or $q_y=0$.

2. Anharmonic energy

The variational Hamiltonian for the (π,π) checkerboard state is of form (2.17) with the matrix given by Eq. (3.14)

$$\mathbf{H}_{\text{var}}(\mathbf{q}) = \alpha_\mathbf{q}\boldsymbol{\eta}\mathbf{V}_\mathbf{q}\mathbf{V}_\mathbf{q}^T\boldsymbol{\eta} + \delta\alpha_\mathbf{q}\mathbf{V}_\mathbf{q}\mathbf{V}_\mathbf{q}^T + \varepsilon\mathbb{1}, \quad (4.8)$$

Diagonalizing $\boldsymbol{\eta}\mathbf{H}_{\text{var}}(\mathbf{q})$, and keeping only the first-order terms in δ, ε results in $\omega_\mathbf{q}$ of order $\sqrt{\varepsilon}$, $\sqrt{\delta}$ along the divergence lines defined by $\beta_\mathbf{q}=0$, and a linear (in ε,δ) correction to $\omega_\mathbf{q}$ away from these lines.

The fluctuations of the variational Hamiltonian are now

$$\mathbf{G}(\mathbf{q}) = \frac{S}{2D_\mathbf{q}(\varepsilon,\delta)}\begin{pmatrix} \alpha_\mathbf{q}(1+\delta)+2\varepsilon & -\gamma_\mathbf{q}(1-\delta) \\ -\gamma_\mathbf{q}(1-\delta) & \alpha_\mathbf{q}(1+\delta)+2\varepsilon \end{pmatrix}. \quad (4.9)$$

Here we defined, for conciseness

$$D_\mathbf{q}(\varepsilon,\delta) \equiv \sqrt{\beta_\mathbf{q}^2(1-\delta)^2 + 4(\alpha_\mathbf{q}+\varepsilon)(\alpha_\mathbf{q}\delta+\varepsilon)}. \quad (4.10)$$

The fluctuations diverge (for nonzero ε) only if $\beta_\mathbf{q}=0$ *and* $\alpha_\mathbf{q}\delta+\varepsilon=0$. If we take $\delta\to-\varepsilon/4$, to conserve the symmetries of the original Hamiltonian, we find one divergent mode: the $\mathbf{q}=0$ Goldstone mode.

In order to calculate the mean-field energy (3.5), we are interested in combinations of the diagonal (on-site) and off-diagonal (nearest-neighbor) fluctuations of the form Γ_{ij}. We can write this as a sum over Fourier modes

$$\Gamma_{ij} = \frac{1}{N_M}\sum_\mathbf{q} \Gamma_{ij}(\mathbf{q}), \quad (4.11)$$

with $\Gamma_{ij}(\mathbf{q})$ defined as

$$\Gamma_{ij}(\mathbf{q}) \equiv G_{l_i l_i}(\mathbf{q}) - \eta_i\eta_j G_{l_i l_j}(\mathbf{q})\cos\vec{\xi}_{ij}\cdot\mathbf{q}. \quad (4.12)$$

Here l_i and l_j are the sublattice indices of i and j, respectively, and $\vec{\xi}_{ij}$ is the vector connecting the two sites. N_M is the number of points in the Brillouin zone, i.e., the number of sites in the magnetic lattice.

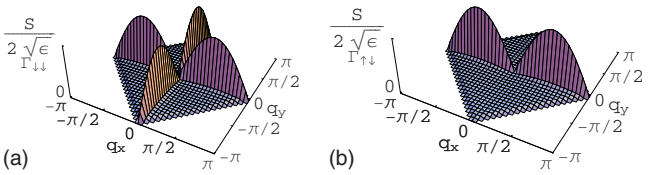

FIG. 3. (Color online) Bond variables in the Brillouin zone of the (π,π) checkerboard state. (a) Γ_{ij} for two neighboring sites on the same sublattice. (b) Γ_{ij} for two neighboring sites with $\eta_i\eta_j=-1$. In the case shown, the (ij) bond is along the x axis. The analytic forms of the functions are given in Eqs. (4.13) and (4.15), respectively.

In this case we obtain, for two neighboring sites on the same sublattice,

$$\Gamma_{\uparrow\uparrow}(\mathbf{q}) = \frac{S}{D_{\mathbf{q}}(\varepsilon,\delta)}[\alpha_{\mathbf{q}}(1+\delta)+2\varepsilon]\sin^2 Q_+, \quad (4.13)$$

$$\Gamma_{\downarrow\downarrow}(\mathbf{q}) = \frac{S}{D_{\mathbf{q}}(\varepsilon,\delta)}[\alpha_{\mathbf{q}}(1+\delta)+2\varepsilon]\sin^2 Q_-. \quad (4.14)$$

Here we used $\Gamma_{\uparrow\uparrow}(\mathbf{q})$ [shown in Fig. 3(a)] for $\Gamma_{ij}(\mathbf{q})$, where both i and j are on the up-spin sublattice (and similarly for $\Gamma_{\downarrow\downarrow}$. For neighboring sites on different sublattices, we obtain [see Fig. 3(b)]

$$\Gamma^{x/y}_{\uparrow\downarrow}(\mathbf{q}) = \frac{S}{2D_{\mathbf{q}}(\varepsilon,\delta)}[\alpha_{\mathbf{q}}(1+\delta)+2\varepsilon-\gamma_{\mathbf{q}}(1-\delta)\cos q_{x/y}], \quad (4.15)$$

where $\Gamma^x_{\uparrow\downarrow}$ ($\Gamma^y_{\uparrow\downarrow}$) is the bond variable for a bond oriented along the x (y) axis, connecting an upspin and a down-spin. Note that Eqs. (4.13)–(4.15) do not diverge at any value of $\mathbf{q}$ for $\varepsilon+4\delta=0$. Thus, we have regularized the fluctuations, and retained only one variational parameter. Since all sites are related by symmetry in this state, $\Gamma_{ij}=\Gamma_{ji}$. Furthermore $\Gamma_{\uparrow\uparrow}(\mathbf{q})$ and $\Gamma_{\downarrow\downarrow}(\mathbf{q})$ are related by a rotation of the Brillouin zone, and the real-space correlations will be the same upon integration over the Brillouin zone.

As we can see in Fig. 3, the divergent lines for $\Gamma_{\uparrow\uparrow}(\mathbf{q})$ and $\Gamma_{\downarrow\downarrow}(\mathbf{q})$ are both major axes, whereas $\Gamma^x_{\uparrow\downarrow}(\mathbf{q})$ and $\Gamma^y_{\uparrow\downarrow}(\mathbf{q})$ only diverge along the y and x axes, respectively. Along the divergent lines, where $\beta_{\mathbf{q}}=0$ and $\alpha_{\mathbf{q}}=|\gamma_{\mathbf{q}}|=4\cos^2 Q_+$, the values of the bond variables are, asymptotically, $\Gamma_{ij}(\mathbf{q})=S|\sin 2Q_+|/2\sqrt{\varepsilon}$. Away from the divergence line,

$$\Gamma_{ij}(\mathbf{q}) \approx \frac{S|\sin 2Q_+|}{2\sqrt{\varepsilon+4q_\perp^2}}, \quad (4.16)$$

where $q_\perp \ll 1$ is transverse to the divergence line. Upon integration of Eqs. (4.13)–(4.15) over the Brillouin zone, the result is a logarithmic singularity in the fluctuations,

$$\Gamma_{\uparrow\uparrow}=\Gamma_{\downarrow\downarrow}=-\frac{4S}{\pi^2}\ln\varepsilon+\mathcal{O}(\varepsilon)=2\Gamma_{\uparrow\downarrow}+\mathcal{O}(\varepsilon). \quad (4.17)$$

Observe that, in the notation of Eq. (3.9), $\Gamma_{\uparrow\uparrow}=\Gamma_{\downarrow\downarrow}=\Gamma^{(0)}+\Gamma^{(2)}$ and $\Gamma_{\uparrow\downarrow}=\Gamma^{(0)}-\Gamma^{(2)}$ so the ratio 2 in Eq. (4.17) is equivalent to the ratio 3 in Eq. (A12). These fluctuations $\{\Gamma_{ij}\}$, divergent as $\ln\varepsilon$, enter quadratically into the anharmonic term of Eq. (3.5) for the mean-field energy E_{MF} (the divergent part of the harmonic contribution, linear in $\{\Gamma_{ij}\}$, cancels as was noted in Sec. III A 2),

$$E_{\mathrm{MF}} = E_{\mathrm{harm}} + S\times\mathcal{O}(\varepsilon) - \sum_{\langle ij\rangle}\eta_i\eta_j(\ln\varepsilon)^2 + \mathcal{O}(\varepsilon\ln\varepsilon),$$

$$= E_{\mathrm{harm}} + S\times\mathcal{O}(\varepsilon) + \frac{4(\ln\varepsilon)^2}{\pi^4} + \mathcal{O}(\varepsilon\ln\varepsilon). \quad (4.18)$$

Minimizing Eq. (4.18) with respect to ε, for a given $S\geqslant 1$ (ignoring the subdominant last term), we obtain $\varepsilon^*(S)\propto \ln S/S$ and therefore the quartic energy $E_{\mathrm{quart}}\equiv E_{MF}-E_{\mathrm{harm}}$ is quadratic in $\ln S$. We remark that due to the logarithmic singularity, in a numerical calculation one would expect it to be hard to distinguish between terms of order $\mathcal{O}(\ln\varepsilon^2)$, $\mathcal{O}(\ln\varepsilon)$, and $\mathcal{O}(1)$ for numerically accessible values of ε. Nevertheless, since we are doing a large-S expansion, we are mostly interested in the asymptotic behavior.

B. Anharmonic ground state selection

Now that we looked at the checkerboard (π,π) state, what can be said about the anharmonic selection in the checkerboard lattice? The harmonic ground states in the checkerboard are the zero-flux state: all of the states that have a positive product over η_i around all square plaquettes.

In this section, we shall first find the ordinary spin-wave modes (ignoring the generic zero modes, which are the same for all states), and then focus on the divergent modes to predict which state is favored. Next, we show some numerical evidence to support are prediction.

1. Spin-wave modes for a generic harmonic ground state

In order to understand the leading-order term in the anharmonic energy, we restrict our discussion to the correlations due to divergent modes. We would like to derive an expression for Γ_{ij}, for any zero-flux state.

We start by explicitly finding the ordinary spin-wave modes of the harmonic Hamiltonian (2.6). Recall that the divergent modes are a subset (of measure zero) of the ordinary modes. Since we expect the divergent and nearly divergent modes to dominate the fluctuations, we shall later limit ourselves to ordinary modes in the vicinity (in $\mathbf{q}$ space) of the divergent modes.

As we saw in Sec. II B 2, any ordinary mode $\mathbf{v}_m$ can be written [Eq. (2.14)] in terms of a vector $\mathbf{u}_m$, of length $N_s/2$, living on the centers of "tetrahedra." In the checkerboard case, these correspond to square lattice sites. $\{\mathbf{u}_m\}$ satisfy the spin-wave equation (2.15), which can easily be solved by an ansatz

$$u_{\mathbf{q}}(\alpha) = \nu_\alpha\sqrt{\frac{2}{N_s}}e^{i\mathbf{q}\cdot\mathbf{r}_\alpha}, \quad (4.19)$$

with $\nu_\alpha=\pm 1$ (to be determined). Plugging this into Eq. (2.15), we obtain, for any α,

$$\lambda_{\mathbf{q}} = \frac{1}{2}\sum_{\beta}^{\text{ord}}{}_{\text{n.n. of } i} \eta_{i(\alpha\beta)}\nu_\alpha\nu_\beta\varepsilon^{i\mathbf{q}\cdot(\mathbf{r}_\beta-\mathbf{r}_\alpha)}. \tag{4.20}$$

As always, "ord" denotes a quantity limited to contributions from ordinary modes. In order for the right-hand side of Eq. (4.20) to be independent of α, we choose

$$\nu_\alpha\nu_\beta = \eta_{i(\alpha\beta)}. \tag{4.21}$$

It is easy to check that for (only) zero-flux states, the signs of $\{\nu_\alpha\}$ can be chosen consistently so that Eq. (4.21) is satisfied. (Note there is no need to assume the state is periodic.) Thus we obtain, from Eq. (4.20), that for any checkerboard-lattice zero-flux state, the dispersion is

$$\lambda_{\mathbf{q}} = 2\cos q_x \cos q_y. \tag{4.22}$$

Note that here q_x and q_y are shifted by $(\pi/2,\pi/2)$ compared to Eq. (4.4) [for the (π,π) state]. This dispersion is shared by all of the harmonic ground states of the checkerboard.

The (normalized) checkerboard-lattice ordinary spin-wave modes are, using Eq. (4.19) in Eq. (2.14), thus

$$v_{\mathbf{q}}(i) = \eta_i\frac{1}{\sqrt{N_s}}\sum_{\alpha:i\in\alpha}\nu_\alpha e^{i\mathbf{q}\cdot\mathbf{r}_\alpha}. \tag{4.23}$$

The first term above vanishes upon summing over the lattice.

2. Divergent correlations

From Eq. (4.23), we can calculate the correlations due to ordinary modes, using Eqs. (2.13) and (2.16),

$$G^{\text{ord}}{}_{ij} = \eta_i\eta_j\sum_{\alpha:i\in\alpha}\sum_{\beta:j\in\beta}\nu_\alpha\nu_\beta\tilde{g}_{\alpha\beta}, \tag{4.24}$$

where

$$\tilde{g}_{\alpha\beta} \equiv \frac{S}{2N_s}\sum_{\mathbf{q}}\frac{\cos\mathbf{q}\cdot(\mathbf{r}_\alpha-\mathbf{r}_\beta)}{|\lambda_{\mathbf{q}}|}, \tag{4.25}$$

is manifestly independent of which (zero-flux) state we have. Remember sum (4.24) has four terms; in the limit of a large system, sum (4.25) converts to an integral in the standard fashion. This is a special case of Appendix A 1: Eq. (4.24) corresponds to Eq. (A2), and Eq. (4.25) corresponds to Eq. (A3) with $\tilde{g}_{\alpha\beta}=\nu_\alpha\nu_\beta g_{\alpha\beta}$.

At this point it appears that we have a problem. The integrand in Eq. (4.25) diverges for any $\mathbf{q}$ along the divergence lines, and therefore, of course, the correlations G_{ii}, G_{ij} diverge for the unperturbed harmonic theory. However, we have found that an adequate regularization scheme, such as variational Hamiltonian (3.14), cuts off the singularity and results in a logarithmic dependence. In particular, we have seen that, for the (π,π) state, $\frac{1}{N_s}\Sigma_{\mathbf{q}}(1/|\lambda_{\mathbf{q}}|)$ can be replaced by a constant $C(\varepsilon)$ which is logarithmic in ε. Since the dispersion of $\lambda_{\mathbf{q}}$ is the same for any zero-flux state, then $C(\varepsilon)$ can be assumed to be the same for all of the harmonic ground states.

Without loss of generality, suppose site i is on the bond between diamond sites α and β and j is shared by α and β'. Plugging this into Eq. (3.3) and using relation (4.21), we find the bond variables,

$$\begin{aligned}\Gamma^{\text{ord}}{}_{ij} &= G^{\text{ord}}{}_{ii} - \eta_i\eta_j G^{\text{ord}}{}_{ij},\\ &= \frac{1}{N_s}\sum_{\mathbf{q}}\frac{S}{2|\lambda_{\mathbf{q}}|}[1-\eta_i\eta_j\cos\mathbf{q}\cdot(\mathbf{r}_\beta-\mathbf{r}_{\beta'})\\ &\quad+\eta_i\cos\mathbf{q}\cdot(\mathbf{r}_\beta-\mathbf{r}_\alpha)-\eta_j\cos\mathbf{q}\cdot(\mathbf{r}_{\beta'}-\mathbf{r}_\alpha)].\end{aligned} \tag{4.26}$$

The last two terms in this expression are identically 0 (since the sum is odd in $\mathbf{q}$), and thus

$$\Gamma^{\text{ord}}{}_{ij} = \frac{1}{N_s}\sum_{\mathbf{q}}\frac{S}{2|\lambda_{\mathbf{q}}|}[1-\eta_i\eta_j\cos\mathbf{q}\cdot(\mathbf{r}_\beta-\mathbf{r}_{\beta'})]. \tag{4.27}$$

Assuming that the anharmonic selection is solely due to nearly divergent modes, we would like to focus on the vicinity of the divergence lines in the Brillouin zone: $q_x \approx \pm\pi/2$ and $q_y \approx \pm\pi/2$.

If the bond (ij) is diagonal, $\mathbf{r}_\beta-\mathbf{r}_{\beta'}=(\pm 2,\pm 2)$, and the integral of the second term over any of the divergence lines is identically zero.[24] On the other hand, for a bond in the $\hat{x}$ [resp. $(\hat{y})$] direction, the bond term in the bracket is $+\eta_i\eta_j$ for $\mathbf{q}=(\pm\pi/2,q_y)$ [resp. $\mathbf{q}=(q_x,\pm\pi/2)$] and 0 otherwise.

Thus we find

$$\Gamma_{ij} \approx \begin{cases} SC(\varepsilon), & (ij)\text{ diagonal bond}\\ SC(\varepsilon)\left(1+\frac{1}{2}\eta_i\eta_j\right), & (ij)\ \hat{\mathbf{x}}\text{ or }\hat{\mathbf{y}}\text{ bond}\\ 0, & \text{otherwise.}\end{cases} \tag{4.28}$$

Comparing to Eq. (3.9), we see that $\Gamma^{(0)}=SC(\varepsilon)$ while $\Gamma^{(2)}=\frac{1}{2}\Gamma^{(0)}$ on $\hat{x}$ or $\hat{y}$ bonds, but zero on diagonal bonds; the form is modified from Eq. (3.9), owing to the anisotropy of the "tetrahedron" in the checkerboard lattice (i.e., the inequivalence of the two kinds of bond.)

Equation (4.28) is by no means an exact result. We have made the following approximations in obtaining it: (i) Neglecting modes away from the divergence lines. This assumption is innocuous for large S since the correlations are dominated by the vicinity of divergent modes. (ii) Neglecting all generic zero modes. In the checkerboard lattice, these modes, close to the divergence lines, can be shown to closely mimic the behavior of the ordinary modes, and will essentially increase $C(\varepsilon)$ by a factor of 2 (see Appendix A 4). (iii) Ignoring any additional effects due to the regularization scheme. Although this assumption is not *a priori* justified, we would like, as a first-order approximation, to work with the bare harmonic Hamiltonian rather than the variational one since it is easier to deal with analytically. We do not expect the regularization to qualitatively change the results we discussed in the following.

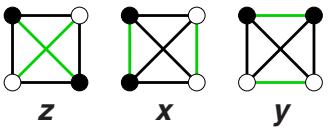

FIG. 4. (Color online) The three possible polarization axes for a single tetrahedron.

3. Single tetrahedron

To find the leading-order quartic energy for a generic state, we consider the three possible bond configurations for a single tetrahedron, which can be viewed as three *polarization axes*:[25,26] z [where all tetrahedra are oriented as in the (π,π) state], x, and y (see Fig. 4).[27]

Summing up the contributions, we obtain, for a single z polarized tetrahedron,

$$E_{\text{quart}}^{\boxtimes} = \frac{1}{S^2} \sum_{\langle ij\rangle \in \boxtimes} \eta_i \eta_j \Gamma_{ij}^2 \approx C(\varepsilon)^2. \tag{4.29}$$

On the other hand, for x or y polarization we find

$$E_{\text{quart}}^{\boxtimes} \approx 2C(\varepsilon)^2. \tag{4.30}$$

Note that in all cases $\Sigma \eta_i \eta_j \Gamma_{ij}^{(m)} \approx 0$ to leading order since the divergent modes do not contribute to the harmonic part of E_{MF} in Eq. (3.5).

Thus we found that the divergent contribution to the quartic energy is twice as large for x or y polarization as it is for z polarization. It follows that the effective Hamiltonian has the simplified form

$$E_{\text{quart}}^{\text{eff}} = N_s[A(S) - B(S)\rho_z], \tag{4.31}$$

with $B(S) \approx A(S)/2$. Therefore the (π,π) state, in which all tetrahedra are z polarized, would be favored over all other zero-flux states, and thus is the *unique* ground state for the checkerboard lattice.

4. Numerics for full lattice

To confirm Eq. (4.31) on the anharmonic selection among harmonic checkerboard ground states, we constructed various such states on a 8×8 cell (see Fig. 5) in the following way: we started from the (π,π) state. There are eight horizontal lines that each go through the centers of four tetrahedra (dashed lines in Fig. 5). We choose any of the 2^8 subsets of these eight lines, and change the sign of $\eta_i \eta_j$ on *every* (vertical or diagonal) bond that crosses one of the chosen horizontal lines. It is easy to check that each of these 2^8 transformations is a valid gaugelike transformation since it does not violate the tetrahedron rule nor does it change the flux through any square plaquette. It turns out that of the 2^8 that can be obtained, only 32 are unique by lattice symmetry. Note that the construction of states, as well as our calculation, is based on bond order,[20] and thus we need not worry about flipping an odd number of lines of this structure.[28] See Ref. 11 for a detailed discussion of gaugelike transformations; for our purpose, it suffices to realize that each state that we generate is a valid classical ground state with zero flux through each plaquette.

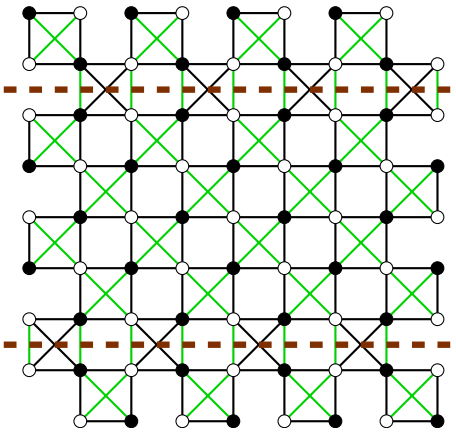

FIG. 5. (Color online) A checkerboard-lattice harmonic ground state. This state was constructed by flipping the bonds that cross each of the two dashed horizontal lines.

Whenever we flip a row of bonds, we change the polarization of four tetrahedra from the z direction to the x direction. Based on the arguments of the previous section, we expect that the leading-order term in the quartic energy would be proportional to the number of flipped rows.

For each of these states, we calculate the quartic energy for a given value of $\varepsilon = 0.001$, integrating over 41×41 points in the Brillouin zone, equivalent to a system size of 328×328, which is more than required to obtain good accuracy (see Sec. V for more details about the numerical considerations). The results are presented in Fig. 6, as a function of the fraction of z-polarized tetrahedra ρ_z. As expected we find: (i) the quartic energy is, for the most part, linear in ρ_z. (ii) the energy span is of order $4(\ln \varepsilon)^2/\pi^4$. (iii) the ground state is the uniformly z polarized (π,π) state. (iv) the quartic energy of the (π,π) state is approximately half of the energy of the uniformly x polarized state.

Given the clear differences in $E_{\text{quart}}(\varepsilon, S)$ between the various harmonic ground states, we expect that the same ordering would be conserved in the saddle-point value $E_{\text{quart}}(S)$ upon minimization with respect to ε. Thus we can claim that the (π,π) state is the zero-temperature large-S ground state of the checkerboard-lattice model. This ground state is the

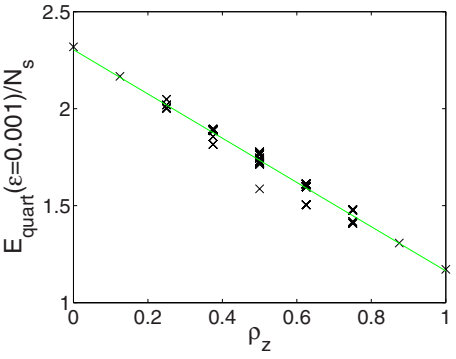

FIG. 6. (Color online) Quartic energy for checkerboard-lattice harmonic ground states. The energy E_{quart} is shown for $\varepsilon = 0.001$, as a function of the fraction of z polarized tetrahedra, for various checkerboard-lattice harmonic ground states.

same one found in large-N calculations for the large-S limit.[10,29] The effective quartic Hamiltonian has the form as Eq. (4.31) with the coefficients $B(S) \propto (\ln S)^2$ and $A(S) \approx 2B(S)$ to leading order in S. We note that this effective Hamiltonian can be written in a more conventional form, in terms of Ising products,

$$E_{\text{quart}}^{\text{eff}} = N_s A(S) - B(S) \sum_{\langle ij \rangle}{}^{\times} \eta_i \eta_j, \tag{4.32}$$

where $\Sigma^{\times}$ is a sum is over diagonal bonds only.

The result is not very surprising: although we set the Heisenberg couplings to be the same for all bonds in the checkerboard lattice, there is no physical symmetry between the diagonal bonds and the nondiagonal bonds and therefore we should have expected to generate anharmonic terms consistent with the actual lattice symmetry. Thus, unfortunately, this does not provide a guide to lattices where all bonds in a tetrahedron are related by symmetry.

V. EFFECTIVE HAMILTONIAN FOR THE PYROCHLORE

We now turn our attention back to the pyrochlore lattice, where, due to the large sizes of the magnetic unit cells of ground state candidates, it would be challenging, at the least, to do analytic calculations (as were done for the checkerboard in Sec. IV). Since Sec. IV explicitly worked out the details, for that case, of implementing the self-consistent framework of Sec. III, we shall not belabor steps which are roughly parallel. However, the selection effects themselves—our ultimate motive—are quite different now since the degeneracy is broken by *ordinary* modes in the checkerboard case.

Our aim here is to calculate the quartic energy for a set of periodic states, and gather the energies we have calculated to construct an effective Hamiltonian. As seen in the harmonic theory of Ref. 11, and in the large-N theory of Ref. 10, as well as the anisotropic perturbation theory of Refs. 30 and 31, it is natural that any non-trivial energy differences among states should be represented as a sum over *loop* operators. The effective Hamiltonian cannot take a local form: the *local* environments that all spins see are the same. [Indeed, if we replaced the diamond lattice by a (loop-free) four-coordinated lattice Bethe, so that our spin sites formed a "Husimi cactus,"[32] then *all* Ising ground states would be equivalent by symmetry.[11]]

The numerical calculation is done as follows: for a given collinear classical ground state and a given value of ε, we diagonalize the Fourier transform of variational Hamiltonian (3.14), keeping $\varepsilon + 4\delta$ infinitesimal. We find the bond variable $\Gamma_{ij}(\mathbf{q})$ for each wave vector on a grid of Brillouin-zone points, and sum over these points to obtain Γ_{ij} in real space. Once we have calculated E_{MF} for many values of ε (for a given collinear state), we can minimize it, for a given S, and find $E_{\text{quart}}(S)$. Our plan of action is to perform this numerical calculation of E_{quart} for a large database of collinear classical ground states and construct an effective Hamiltonian.

A. Logarithmic divergences

In performing the calculation, we find a distinct resemblance to our findings on the checkerboard lattice: There are divergent modes along the x, y, and z axes in the Brillouin zone,[11] and these modes dominate the mean-field quartic energy (and have no contribution to the harmonic-order energy). The singularity of $\Gamma_{l_i l_j}(\mathbf{q})$ is cut off, along the divergence lines, by a term of the order $S/\sqrt{\varepsilon}$. The divergence peaks drop off to half of their maximum value at a $(\mathbf{q})$ distance of order $\sqrt{\varepsilon}$, away from the divergence line. This means that the grid of wave vectors that we use must be denser in order to capture the effect of the divergent modes, as ε becomes smaller. Thus, we need to sum of the order of $\varepsilon^{-3/2}$ points, to obtain good accuracy. This limits the values of S that we can do the calculation for, and we have found no useful numerical tricks to get around it. Nevertheless, we can get results over about two orders of magnitude of S, which can be extrapolated to the $S \to \infty$ limit.

Upon numerical integration, we find, that as in the two-dimensional checkerboard lattice, the divergence of the fluctuations is logarithmic,

$$\Gamma_{ij} \propto |\ln \varepsilon| + \mathcal{O}(\varepsilon). \tag{5.1}$$

This numerical finding is somewhat surprising. We would naively expect that the bond variable $\Gamma_{ij}(\mathbf{q})$ would drop, away from the divergent lines, with functional form (4.16), as in the checkerboard. If so, as the transverse integration over $\mathbf{q}_\perp$ is now two dimensional, the result would be a nonsingular Γ_{ij}.

It turns out that this expectation is incorrect because the dispersion in the direction perpendicular to the divergence line is strongly anisotropic. For each value of $\mathbf{q}$ along the divergence line, there are two particular independent eigendirections of $\mathbf{q}_\perp$. For example, for a $\mathbf{q}=q_z\hat{\mathbf{z}}$ divergence, the eigendirections of $\mathbf{q}_\perp$ are (1,1,0) and (1,−1,0). If we call unit vectors along these eigendirections $\hat{\mathbf{e}}_1$ and $\hat{\mathbf{e}}_2$, then we find that $\Gamma_{ij} \propto 1/\sqrt{\varepsilon + (q_\perp \cdot \hat{\mathbf{e}}_1)^2} + 1/\sqrt{\varepsilon + (q_\perp \cdot \hat{\mathbf{e}}_2)^2}$. Integration over $\mathbf{q}_\perp$ results in the logarithmic dependence on ε of Eq. (5.1), as in the checkerboard case. In turn, as in Sec. IV A 2, the logarithmic scaling of fluctuations in Eq. (5.1) implies via Eq. (3.18) that

$$\varepsilon^*{}_{\text{SC}}(S) \propto \frac{\ln S}{S}. \tag{5.2}$$

Finally, we know the decoupled quartic energy in Eq. (3.5) is a sum over products $\Gamma_{ij}\Gamma_{ji}$, with Γ_{ij} linear in $\ln S$; since the divergent parts linear in Γ_{ij} cancel out [as noted before Eq. (A11)], the result is the anharmonic energy scales as $(\ln S)^2$, as announced in Eq. (3.23).

B. Gauge-invariant terms

For our database we calculated E_{quart} on a sample of classical ground states (not all of them π-flux states), which we constructed by hand, with unit cells ranging from four to 32 sites. Two of these families consist of the zero-flux and π-flux states, which have uniform +1 and −1 products around all hexagons, respectively. In the other three gauge families, the hexagon fluxes are arranged in planes such that within each plane the flux is uniform; we call these the "000π," "0π0π," and "00$\pi\pi$" plane states, according to the stacking sequence.

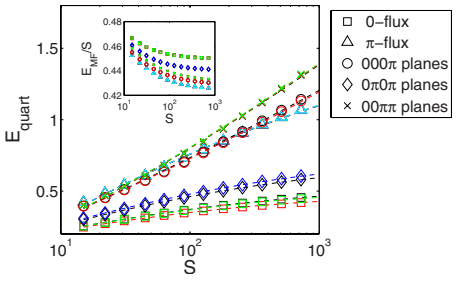

FIG. 7. (Color online) Quartic energy E_{quart} for 16 classical collinear ground states. $E_{\text{quart}}(S)$ was obtained in the variational calculation. The lines show a numerical quadratic fit in $\ln S$. Each gauge family (represented by two to six different states each) is denoted by a different symbol, of which triangles denote the harmonic ground states—the π-flux states. We show six π-flux states, and their energies are virtually indistinguishable to the naked eye. The total energy E_{MF} is shown in the inset.

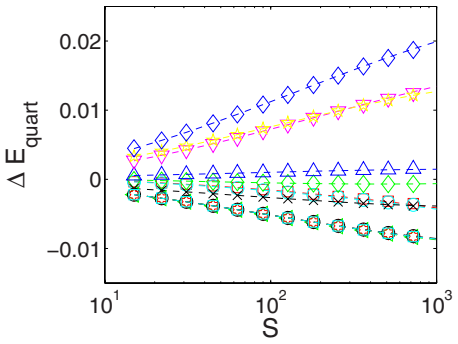

FIG. 8. (Color online) Energy difference between E_{quart} of 12 harmonic ground states and the average of their energies $\bar{E}_{\text{quart}}$. By taking differences between energies, we eliminate the (dominant) gauge-invariant term in the anharmonic energy. Each dashed line shows a fit in $\ln S^2$, for one of the states. Note that there are several overlapping symbols along the bottom line, representing the degenerate states described later in the text (those with the maximum possible value of $\mathcal{P}_6=N_s/3$).

We minimize the E_{MF} with respect to ε at each value of S and obtain the energy shown in the inset of Fig. 7. We focused on the five simplest gauge families. We minimize the E_{MF} with respect to ε at each value of S and obtain the energy shown in the inset of Fig. 7. We focused on the five simplest gauge families. We show the energies of all 16 distinct Ising states belonging to the five gauge families. Due to the exact invariance of the ($\varepsilon=0$) harmonic energy under the gaugelike transformation, the total energies of states related by such transformations are, as expected, indistinguishable in the inset since the harmonic term dominates.

In the main part of Fig. 7 we show the anharmonic energy E_{quart} for the same states. As in the checkerboard lattice, the dominant part of the quartic energy is quadratic in $\ln S$, and of the order $(\ln S)^2$. However, unlike the checkerboard lattice (compare to Fig. 6), we find that the energy *differences* between harmonically degenerate states are one to two orders of magnitude smaller than the dominant quartic energy.

We first consider the dominant gauge-invariant contribution to the quartic energy. Since the invariants of the gaugelike transformation are products around loops, we search for an effective Hamiltonian in terms of the fluxes Φ_{2n}, similar to the harmonic effective Hamiltonian (1.5),

$$E_{\text{quart}}^{\text{eff}} = A_0 + A_6(S)\Phi_6 + A_8(S)\Phi_8 + A_{10}(S)\Phi_{10} + \cdots, \tag{5.3}$$

where we find, numerically,

$$A_0(S) \approx 0.300 + 0.0130(\ln S)^2,$$

$$A_6(S) \approx -0.116 - 0.0030(\ln S)^2,$$

$$A_8(S) \approx -0.022 + 0.0055(\ln S)^2,$$

$$A_{10}(S) \approx 0.008 - 0.0021(\ln S)^2. \tag{5.4}$$

Note that for large S, the signs of the coefficients A_6, A_8, and A_{10} are opposite to K_6, K_8, and K_{10} in the harmonic Hamiltonian. The differences in signs among the $A_l(S)$ coefficients can explain why some of the lines in Fig. 7 appear to be convex and other concave: each family of states is dominated by different flux loop lengths l.

The gauge-invariant terms can be heuristically explained in terms of the divergent modes: the quartic energy is large for states that have a large number of divergent modes. It turns out[11,20] that the number of divergent modes is linearly related to the flux terms Φ_{2n}: divergent modes proliferate to the extent that the fluxes through loops of length $2n$ are $(-1)^n$.

The above discussion of the gauge-invariant quartic energy (5.3) is somewhat moot, inasmuch as it is negligible compared to harmonic energy (1.5), and it does not break the gaugelike symmetry. Nevertheless, one can clearly see in Fig. 7 that the anharmonic energy within each gauge family is not exactly the same, meaning that there is a gauge-dependent term in the variational anharmonic energy.

C. Gauge-dependent terms and effective Hamiltonian

Upon close inspection of Fig. 7, we see that some of the gauge families have a larger dispersion in their quartic energies than others. But the quartic energy differences among the ground states of the harmonic Hamiltonian—the π-flux states—are much smaller than the gauge-invariant contribution. We attribute this to the fact that, unlike the checkerboard-lattice harmonic ground states or even some pyrochlore gauge families, the π-flux states are completely uniform and isotropic (at the gauge-invariant level), and therefore there is no reason for the harmonic degeneracy to be broken at the single- tetrahedron level (see the discussion of Sec. IV B 3). Indeed, in Appendix A we show that the quartic energy due to *ordinary* modes of $\mathcal{H}_{\text{harm}}$—the dominant contribution—is gauge invariant among π-flux states. (This was not the case for the checkerboard case of Sec. IV B.) We would expect any gauge-dependent terms in an effective Hamiltonian to not be as local as those in, say, Eq. (4.31).

In Fig. 8, we zoom in on the gauge-dependent anharmonic

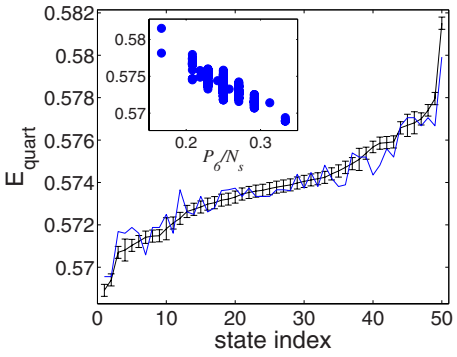

FIG. 9. (Color online) The points with error bars are the numerical result E_{quart} ($S=100$) for 50 distinct π-flux states, which had been found using our algorithm for generating gaugelike transformations. (Note that these energies are monotonic by construction, as the "state index" means simply the sequence when these energies are sorted. Every seventh energy is plotted. Shown for comparison are the energies predicted by quartic effective Hamiltonian (5.5), using best-fit values for the three coefficients. The inset shows E_{quart} ($S=100$) as a function of the effective Hamiltonian's leading term, $\mathcal{P}_6$.

energy, by showing the difference $\Delta E_{\text{quart}} \equiv E_{\text{quart}} - \bar{E}_{\text{quart}}$, where E_{quart} is calculated for 12π-flux states, and $\bar{E}_{\text{quart}}$ is the mean quartic energy of the states shown in the plot.

In order to systematically search for a ground state configuration of the anharmonic effective Hamiltonian, we constructed a large number of harmonic ground states using an algorithm for randomly generating gaugelike transformations.[11] Within unit cells that we used, of up to 192 sites, we believe that the algorithm performs an *exhaustive* search for harmonic ground states. About 350 states were found, inequivalent by lattice symmetries. (Notice that noncubic cells were tried; indeed, the optimal states described below require a cell dimension that is a multiple of $3a/4$ in the stacking direction.)

The overall anharmonic energy (see Sec. III C) depends on S as $(\ln S)^2$, as does its gauge-invariant part [see Eq. (5.4)]; is this also true for the gauge-dependent selection terms we seek? From what has been shown so far, that would be a plausible conjecture based on the scaling of the total energy, as well as the checkerboard case. Empirically, for each of our harmonic ground states, the S dependence of its energy (including the gauge-dependent part) is well fitted by a linear or quadratic function $\ln S$ (as seen in Fig. 8). In fact, the checkerboard case is misleading: the anharmonic selection there (unlike the pyrochlore) depends on the ordinary spin-wave modes. The analytic derivation in Sec. VI shows the gauge-dependent term actually should scale as $\ln S/S$; we do not understand the discrepancy between this and the numerical results.

In Fig. 9 we plot E_{quart} for the harmonic-order ground states at $S=100$. There are two sources of error in this calculation: The first is the minimization error, represented by the error bars, which is due to the difference in energy between consecutive value of ε that we calculated, i.e., due to the "grid" in ε-space. The second source of error is the grid used in integrating over the Brillouin zone, which is equivalent to a finite (albeit large) system size. This error becomes more significant for large values of S (i.e., smaller values of ε), where the singularity of the divergence lines becomes narrower. The results shown are for 15^3 points in the Brillouin zone, for two different magnetic unit cells: a cubic 128 site unit cell, and a 96 site tetragonal unit cell.

As noted at the beginning of this section, we anticipate that an effective Hamiltonian should be represented by some sort of loop variables. We now consider an effective Hamiltonian of the form

$$\Delta E^{\text{eff}}_{\text{quart}} = C_6(S)\mathcal{P}_6 + C_8(S)\mathcal{P}_8 + C_{10}(S)\mathcal{P}_{10}, \tag{5.5}$$

where $\mathcal{P}_l$ is equal to the number of loops of length l composed solely of satisfied AFM bonds. The form (5.5) was partly inspired by the effective Hamiltonian from Ref. 10, which is also a count of alternating loops (but with a broader definition of "loop" than here). Equation (5.5) was guessed after fitting other forms with a variety of two- and four-spin terms involving the several closest neighbors. [Due to the ground state constraint $\Sigma_{i\in\alpha}\ \eta_i=0$ and the π-flux constraint (1.4), there are numerous linear dependencies among such terms.]

Also shown in Fig. 9 is a numerical fit to the effective Hamiltonian (5.5). For $S=100$ we obtain

$$C_6 = -0.0621,$$

$$C_8 = -0.0223,$$

$$C_{10} = -0.0046. \tag{5.6}$$

We ignore any constant terms here, as they belong in the gauge-invariant Hamiltonian (5.3).

While we cannot numerically repeat this calculation over a large range of values of S, in order to find the functional dependence $C_l(S)$ with good accuracy, we can obtain a rough fit by considering the small group of states depicted in Fig. 8. For these 12 states we obtain

$$C_6(S) \approx -0.015 - 0.004(\ln S)^2 \approx 0.05 - 0.03 \ln S,$$

$$C_8(S) \approx 0.002 - 0.002(\ln S)^2 \approx 0.04 - 0.02 \ln S,$$

$$C_{10}(S) \approx 0.0008 - 0.0005(\ln S)^2 \approx 0.009 - 0.004 \ln S. \tag{5.7}$$

Over our range of $S=10$ to 1000, either fit is plausible but $\ln S$ is a little better than $(\ln S)^2$.

It must be noted that (at $S=100$) the coefficients in Eq. (5.7) are bigger than Eq. (5.6) by nearly a factor of two; this is because the 12 states used were not sufficiently representative. Even though it is a rough fit, with significant error, it is clear (see the inset in Fig. 9) that for a large number of states, the leading-order contribution to the energy is captured in Eq. (5.5). In particular, the numerical energy and the effective Hamiltonian agree as to which states have the minimum and maximum energies. As it turns out, this can be predicted from the first term in Eq. (5.5): the highest energy states are those with the highest $\mathcal{P}_6$ value, namely, $N_s/6$, which means $1/6$ of all hexagons have alternating spin di-

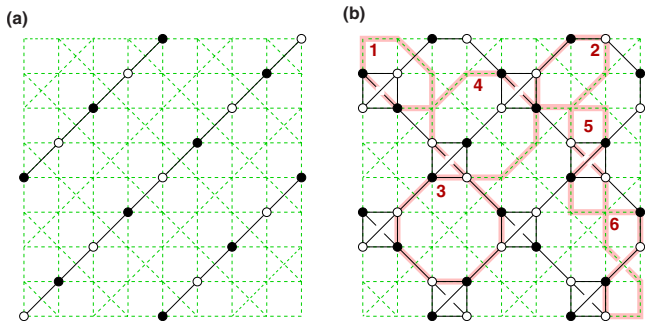

FIG. 10. (Color online) Projection of the slabs which form the near-degenerate anharmonic ground states of $\mathcal{P}_6$, showing A layer in (a) and B layer in (b). The square shown is $2a\times 2a$. Open and filled circles represent spin up and down. Dashed lines are bonds outside the slab. In (b), one loop is outlined (numbered) from each of the two classes of hexagon mentioned in text and in Table I; there are also four classes for octagon placement, numbered 3–6 here.

rections. It can be shown that, for π-flux states, this is the smallest value that $\mathcal{P}_6$ can take.[20] The lowest energy states have $\mathcal{P}_6=N_s/3$ which is the highest possible value of $\mathcal{P}_6$.

D. Ground states

Since the $\mathcal{P}_6$ term is largest, and in view of the results just mentioned, it is a reasonable guess that the ground states are a subset of the "hexagon ground states" that maximize just the $\mathcal{P}_6$ term. Since (see Appendix C 1) all hexagon ground states are degenerate at the octagon term too, only the much weaker ten-loop term might split these states, this assumption—confirmed numerically in the results of Sec. V C—is very plausible.

All hexagon ground states found could be constructed by layering two-dimensional slabs (see Fig. 10); they had unit cells of 48 spins (or larger). They were, within the numerical accuracy that we can obtain, degenerate for all values of S. In fact, we found these states share the same values of $\mathcal{P}_l$ for all loop lengths that we calculated ($l\leqslant 16$). Appendix B explains these facts: indeed, it is shown that all loops are identical for $l<26$, and hence the stacked hexagon ground states must be *exactly* degenerate up to that order, at least for any effective Hamiltonian written in terms of loops [whether of the form (5.5) or the form to be derived in Sec. VI].

We conjecture that the stackings are, in fact, the only ground hexagon ground states, but this is unproven since we have not tried all possible unit-cell shapes in the numerical enumeration. Appendix C explains how one could approach the ground state problem as a color-matching problem, but does not solve it.

Although we shall find a different version of the effective Hamiltonian in Sec. VI, this section is valid for that too. All that matters is that the effective Hamiltonian depends on the Ising configurations of loops, and that the hexagon term dominates.

VI. LOOP EXPANSION

In Sec. III we saw that in our self-consistent theory, the mean-field Hamiltonian is proportional to the variational Hamiltonian

$$\mathcal{H}_{\mathrm{MF}}=J^*\mathcal{H}_{\mathrm{var}}. \tag{6.1}$$

In fact, it turns out that the quartic selection effects of $\mathcal{H}_{\mathrm{MF}}$ can be seen in the zero-point energy of $\mathcal{H}_{\mathrm{var}}$, i.e., J^* does not affect the selection. Therefore, we can try to understand the origin of the quartic effective Hamiltonian (5.5), by studying E_{var}, the zero-point energy of the variational Hamiltonian (3.14), treated as a purely harmonic problem.

In Refs. 9 and 11 we developed an effective Hamiltonian for the harmonic zero-point energy by a real-space loop expansion. Below (Sec. VI B), we shall use the same method as motivation for Eq. (5.5). First, in Sec. VI A, we shall give a quick summary of the results on $\mathcal{H}_{\mathrm{harm}}$. Next, we represent the variational Hamiltonian in similar matrix notation, and repeat the loop expansion (for the leading order in ε), to derive an analytic effective Hamiltonian (Sec. VI C). In Sec. VI D we discuss the obtained effective Hamiltonian and compare it to the effective Hamiltonian we used in the numerical fit.

A. Bare harmonic theory

For this quick review of Ref. 11, it will be convenient to rewrite some results of Sec. II B using the matrix notation of Eq. (2.6), as we note in each place.

The spin-wave modes in the unperturbed harmonic theory are the eigenvectors of the equation [equivalent to Eq. (2.9)]

$$\boldsymbol{\eta}\mathbf{H}\mathbf{v}_m=\lambda_m\mathbf{v}_m, \tag{6.2}$$

where $\mathbf{H}$ can be written as [equivalent to Eq. (2.7)]

$$\mathbf{H}=\frac{1}{2}\mathbf{W}^\dagger\mathbf{W}. \tag{6.3}$$

$\mathbf{W}$ is a $N_s/2\times N_s$ matrix whose (α,i) element is 1 if the pyrochlore site i is in tetrahedron α and zero otherwise.

The spin-wave equation is transformed to the diamond lattice (which is easier to deal with, since it has fewer loops), by defining $\mathbf{u}_m\equiv\mathbf{W}\mathbf{v}_m$. The diamond-lattice modes satisfy the equation [equivalent to (2.14)]

$$\boldsymbol{\mu}\mathbf{u}_m=\lambda_m\mathbf{u}_m, \tag{6.4}$$

with the matrix $\boldsymbol{\mu}\equiv\frac{1}{2}\mathbf{W}\boldsymbol{\eta}\mathbf{W}^\dagger$.

The elements of $\boldsymbol{\mu}$ only connect diamond-lattice nearest neighbors and are equal to the value of η at the center of the bonds,

$$\mu_{\alpha\beta}=\begin{cases}\eta_{i(\alpha\beta)} & \alpha,\beta \text{ nearest neighbors}\\ 0, & \text{otherwise.}\end{cases} \tag{6.5}$$

As before, $i(\alpha\beta)$ is the pyrochlore site at the center of the diamond bond $(\alpha\beta)$. The zero-point energy is $S\Sigma|\lambda_m|$, or in matrix notation

$$E_{\mathrm{harm}}=S\mathrm{Tr}\left(\frac{1}{4}\boldsymbol{\mu}^2\right)^{1/2}-SN_s. \tag{6.6}$$

For each α, the diagonal element $(\frac{1}{4}\mu^2)_{\alpha\alpha}$ is equal to 1, and thus the square root can formally be Taylor expanded in powers of $\boldsymbol{\mu}^2$ (or more exactly of $\boldsymbol{\mu}^2-4\mathbb{1}$),

$$E_{\text{harm}}/S = 1 + \sum_{n=1} Q_{2n}\text{Tr}(\boldsymbol{\mu}^{2n}) - N_s, \tag{6.7}$$

where the coefficients are

$$Q_{2n} \equiv (-1)^{n+1}\frac{(2n-3)!!}{8^n n!}. \tag{6.8}$$

The details of the expansion were given in Ref. 11, where effective Hamiltonian (1.5), written in terms of $\{\eta_i\}$, was derived from Eq. (6.7). However, the harmonic-order selection can be explained with a "back-of-the-envelope" argument, as in Ref. 9: Tr $\boldsymbol{\mu}^{2n}$ is a sum of products of $\eta_{\alpha\beta}$ over all closed paths in the diamond lattice. Since any path that goes back and forth is independent of $\{\eta_i\}$, the only paths that contribute nontrivial terms to the effective Hamiltonian are actual loops in the lattice. The first of these terms in for $n=3$ (corresponding to hexagons in the pyrochlore lattice). Thus, the first nontrivial term in the expansion favors states with negative hexagon fluxes—the π-flux states with $\Pi_{i\in\hexagon}\eta_i=-1$ [Eq. (1.4)].

B. Variational Hamiltonian

The self-consistent theory (Sec. III) employs a variational Hamiltonian which has the same form as the harmonic Hamiltonian but with $\mathbf{H}$ replaced by

$$\mathbf{H}_{\text{var}} = \mathbf{H} - \frac{1}{4}\varepsilon\boldsymbol{\eta}\mathbf{H}\boldsymbol{\eta} + \varepsilon\mathbb{1} \tag{6.9}$$

[to repeat Eqs. (3.14) and (3.17)]. Here $\varepsilon>0$ is the (small) variational parameter. The quartic energy is not equal to, but proportional to, the zero-point energy of the variational Hamiltonian [with its parameter ε^* satisfying self-consistency equation (3.18)]. Let us try to derive an expansion for this energy.

The spin-wave modes are eigenvectors of the equation

$$\lambda_m\mathbf{v}_m = \boldsymbol{\eta}\mathbf{H} - \frac{1}{4}\varepsilon\mathbf{H}\boldsymbol{\eta} + \varepsilon\boldsymbol{\eta}\mathbf{v}_m. \tag{6.10}$$

Replacing $\mathbf{H}$ by Eq. (6.3), we obtain

$$\lambda_m\mathbf{v}_m = \left(\frac{1}{2}\boldsymbol{\eta}\mathbf{W}^\dagger\mathbf{W} - \frac{1}{8}\varepsilon\mathbf{W}^\dagger\mathbf{W}\boldsymbol{\eta} + \varepsilon\boldsymbol{\eta}\right)\mathbf{v}_m. \tag{6.11}$$

Clearly, the recipe for transposing this to the diamond lattice must be generalized to a more complex form than before (which must reduce to the old formulas in the case $\varepsilon=0$). Luckily, thanks to the simple form we adopted for variational Hamiltonian (3.14) it will suffice to expand the vector space of diamond modes from one to two components. Define the two vectors

$$\mathbf{u}^1_m \equiv \mathbf{W}\mathbf{v}_m, \quad \mathbf{u}^2_m \equiv \mathbf{W}\boldsymbol{\eta}\mathbf{v}_m. \tag{6.12}$$

For the case of $\varepsilon=0$, $\{\mathbf{u}^1_m\}$ corresponds to ordinary modes and $\{\mathbf{u}^2_m\}$ to generic zero modes.

It is convenient to introduce, analogous to $\boldsymbol{\mu}$, $\boldsymbol{\nu}\equiv\mathbf{W}\mathbf{W}^\dagger$; thus $\boldsymbol{\nu}$ is independent of $\{\eta_i\}$ and has nonzero elements on the diagonal (with respect to the diamond-site index),

$$\nu_{\alpha\beta} = \begin{cases} 4, & \alpha=\beta \\ 1, & \alpha,\beta \text{ nearest neighbors} \\ 0, & \text{otherwise}. \end{cases} \tag{6.13}$$

Still defining $\boldsymbol{\mu}$ as in Eq. (6.5), we find [by multiplying Eq. (6.11) from the left by $\mathbf{W}$ and $\mathbf{W}\boldsymbol{\eta}$] the new equation of motion,

$$\lambda_m\begin{pmatrix}\mathbf{u}^1_m\\ \mathbf{u}^2_m\end{pmatrix} = \mathbf{M}\begin{pmatrix}\mathbf{u}^1_m\\ \mathbf{u}^2_m\end{pmatrix}, \tag{6.14}$$

with the $2N_s\times 2N_s$ matrix $\mathbf{M}$ defined as

$$\mathbf{M} \equiv \begin{pmatrix} \boldsymbol{\mu} & -\frac{1}{4}\varepsilon(\boldsymbol{\nu}-8\mathbb{1}) \\ \boldsymbol{\nu}+2\varepsilon\mathbb{1} & -\frac{1}{4}\varepsilon\boldsymbol{\mu} \end{pmatrix}. \tag{6.15}$$

The zero-point variational energy is

$$E_{\text{var}} = S\text{Tr}\left(\frac{1}{4}\mathbf{M}^2\right)^{1/2} - SN_s. \tag{6.16}$$

Note that now twice as many elements are summed in the trace as were in the bare harmonic version (6.6). One way to understand this is that the generic zero modes no longer have zero frequency and must explicitly appear in the zero-point sum $S\Sigma|\lambda_m|$.

C. Expansion of variational energy

The square root of Eq. (6.16) can be formally expanded in exactly the sum (6.7), but with the replacement $\boldsymbol{\mu}^{2n}\to\mathbf{M}^{2n}$. In this trace expansion, each factor of $\boldsymbol{\mu}$ or $\boldsymbol{\nu}$ hops us to a neighboring site—with or without a factor of $\eta_i\eta_j$, respectively—whereas a factor of $\mathbb{1}$ does nothing. We expect the lowest-order nontrivial terms in the expansion to be of order six in $\boldsymbol{\mu}$, $\boldsymbol{\nu}$ since it takes (at least) that many hops to complete a hexagon, which is the smallest loop (in the pyrochlore lattice); these contributions come from the $+\text{Tr}(\mathbf{M}^6)$ term

Furthermore, since ε is a small parameter, we shall expand the results in orders of ε, keeping only the lowest-order nontrivial term. Notice that for every $\mathbb{1}$ factor in Eq. (6.15), we pay the price of one power of ε but do not gain a hop: hence, factors of $\mathbb{1}$ cannot ever appear in a *leading* contribution. Such factors serve to "decorate" a basic loop so that the same contribution reappears coming from higher powers of $\mathbf{M}$ and of higher order in ε. They play a role similar to (and in addition to) the decorations by hops that retrace themselves, as found already in the bare harmonic theory.[11]

The upper-left block of $\mathbf{M}$ corresponds to $\{\mathbf{u}^1_m\}$—the ordinary modes, whereas the lower-right block corresponds to $\{\mathbf{u}^2_m\}$—generic zero modes (that acquire nonzero frequency in the variational Hamiltonian). Since the matrix elements of the $\mathbf{u}^2$ sector always carry a factor ε, the leading-order terms in the small-ε expansion will involve hops from the ordinary-mode sector to the zero-mode sector and quickly return back. In this fashion, as conjectured in Appendix A, we shall find explicitly that degeneracy-breaking effects are

due to the interaction between generic zero modes and ordinary modes.

All nonzero terms in a trace represent paths $\mathcal{W}$ of length $2l \leqslant 2n$ on the diamond lattice that start and end on the same site (possibly retracing some bonds); also, $2n-2l$ is the number of factors $\nu_{\alpha\alpha}$ which are diagonal with respect to sites. From here on we imagine having selected a particular path $\mathcal{W}$, which can be expressed as a sequence of pyrochlore sites (diamond-lattice bonds) $(i_1, i_2, \ldots, i_{2l})$; all terms in the traces must be polynomials in the spins $\eta_{i_1}, \eta_{i_2}, \ldots$. Then we considering the terms due to $\mathrm{Tr}(\mathbf{M}^{2n})$ at each order in ε.

The leading-order $[\mathcal{O}(1)]$ terms involve only the upper-left block (ordinary modes) of $\mathbf{M}$. But it will be helpful to notice that $\mathrm{Tr}(\boldsymbol{\mu}^{2n}) = (2n)\varphi_{\mathcal{W}}$, where $\varphi_{\mathcal{W}} \equiv \Pi_{j=1}^{2n} \eta_{i_j}$, which generalizes Eq. (1.3), to a general closed path. (Here the factor $2n$ accounts for different cyclic permutations inside the trace, i.e., different places the same loop could have been started. Note that any retraced portions in $\mathcal{W}$ have canceling contributions in the product $\varphi_{\mathcal{W}}$.) They are clearly gauge-invariant (See Appendix A 2) by the definition of the gauge-symmetry as described in Sec. I A and are in fact exactly the same terms $(\boldsymbol{\mu}^{2n})$ that we had in the bare harmonic theory [Eq. (6.7)]. Such terms in the effective Hamiltonian give the same value for all gauge-equivalent states, so they do not split the harmonic-order degeneracy and are not of interest here.

In the next order, $\mathcal{O}(\varepsilon)$, we can have terms that take us out of the ordinary-mode sector in M and into the zero-mode sector, but come immediately back. We obtain

$$-\frac{1}{2} S n Q_{2n} \varepsilon \mathrm{Tr}[\boldsymbol{\mu}^{2n-2}(\boldsymbol{\nu} - 8\mathbb{1})\boldsymbol{\nu}], \tag{6.17}$$

with the same $2n$ factor for cyclic permutations. The trace in Eq. (6.17) contains two types of terms: Firstly, taking the *site-diagonal* $(\alpha=\beta)$ element in each $\boldsymbol{\nu}$, we obtain $4\varphi_{\mathcal{W}}$ (where $|\mathcal{W}| = 2n-2$.) As noted above, this is gauge invariant hence not of interest.

Secondly, taking the site-*nondiagonal* elements of $\boldsymbol{\nu}$, we obtain a products of all spins except two adjacent ones, i.e.,

$$\varphi_{\mathcal{W}} \sum_j \eta_{i_j} \eta_{i_{j+1}}, \tag{6.18}$$

where we adopted the notation convention $\eta_{i_{j+2n}} \equiv \eta_{i_j}$. In (only) the special case of a π-flux state, all products $\varphi_{\mathcal{W}}$ along paths of the same topology are the same, and therefore a sum over *all* paths of length $2n$ amounts to a multiple of the classical energy $\Sigma_{\langle ij \rangle} \eta_i \eta_j$, and does not split any degeneracies. [More generally, within a family of non-π-flux states, such terms do split the degeneracy and we must keep them. This is probably the reason that the dispersion of quartic energies among non-π-flux states is notably larger than in the π-flux or 0-flux states (see Fig. 7).]

Moving on to the terms of order ε^2, we have contributions (i) from paths that hop once into the zero-mode sector (possibly staying there for at most one hop) and (ii) paths that hop twice into the zero-mode sector (each time hopping back immediately),

$$\frac{1}{8} S n Q_{2n} \varepsilon^2 \Bigg\{ \mathrm{Tr}[\boldsymbol{\mu}^{2n-3}(\boldsymbol{\nu} - 8\mathbb{1})\boldsymbol{\mu}\nu - 4\boldsymbol{\mu}^{2n-2}(\boldsymbol{\nu} - 8\mathbb{1})] + \frac{1}{2} \sum_{m=0}^{2n-4} \mathrm{Tr}[\boldsymbol{\mu}^m (\boldsymbol{\nu} - 8\mathbb{1})\boldsymbol{\nu}\boldsymbol{\mu}^{2n-4-m}(\boldsymbol{\nu} - 8\mathbb{1})\boldsymbol{\nu}] \Bigg\}. \tag{6.19}$$

The prefactor of $1/2$ in front of the second trace corrects the counting factor $2n$ since each placement of the pair of $\boldsymbol{\nu}\boldsymbol{\nu}$ factors is counted twice in the sum.

We now study Eq. (6.19), seeking to keep gauge-dependent terms only. Start with the second term in the first trace, inside the curly brackets: $-4\boldsymbol{\mu}^{2n-2}(\boldsymbol{\nu} - 8\mathbb{1})$. In this term, only the site-diagonal elements in $\boldsymbol{\nu} - 8\mathbb{1}$ can contribute since the path has to be of an even length. By the same arguments given above we just obtain $(-4)(4-8)\varphi_{\mathcal{W}}$ which is gauge invariant. Next, the first term in the first trace in Eq. (6.19) produces one gauge-invariant term (for diagonal elements of $\boldsymbol{\nu}$) plus one term that is gauge dependent,

$$\varphi_{\mathcal{W}} \sum_{k=1}^{2n} \eta_{i_k} \eta_{i_{k+2}} \equiv \varphi_{\mathcal{W}} T_{\mathcal{W}}. \tag{6.20}$$

Every factor inside the trace involves a hop to a different site. Similarly, the sum over traces in Eq. (6.19) results, for a path $\mathcal{W}$, in terms

$$\varphi_{\mathcal{W}} \frac{1}{2} \sum_{j=1}^{2n} \sum_{k=j+2}^{2n+j-2} \eta_{i_j} \eta_{i_{j+1}} \eta_{i_k} \eta_{i_{k+1}}, \tag{6.21}$$

plus gauge-invariant terms that result from diagonal elements in $\boldsymbol{\nu} - 4\mathbb{1}$. This can be simplified into $\frac{1}{2}\varphi_{\mathcal{W}}(U_{\mathcal{W}}^2 - 2T_{\mathcal{W}})$, where we define

$$U_{\mathcal{W}} \equiv \sum_{k=1}^{2n} \eta_{i_k} \eta_{i_{k+1}}. \tag{6.22}$$

Merging these two expressions together, we obtain, up to gauge-invariant terms,

$$\frac{1}{16} S n Q_{2n} \varepsilon^2 \sum_{|\mathcal{W}|=2n} \varphi_{\mathcal{W}} U_{\mathcal{W}}^2. \tag{6.23}$$

It is easy to see that only actual loops contribute interesting terms to Eq. (6.23)—all paths that go back and forth along the lattice add up to terms that are equal for all states that obey the "tetrahedron rule" $\Sigma_{i \in \alpha} \eta_i = 0$. Thus the anharmonic energy, to order ε, can be expressed as a sum over lattice loops $\{\mathcal{L}\}$,

$$E_{\mathrm{var}}(\text{gauge dep.}) = \frac{\varepsilon^2 S}{16} \sum_{n=3} n \widetilde{Q}_{2n} \sum_{|\mathcal{L}|=2n} \varphi_{\mathcal{L}} |U_{\mathcal{L}}|^2 + \mathcal{O}(\varepsilon^3). \tag{6.24}$$

Here, the coefficient $\widetilde{Q}_{2n}$ is not quite the same as Q_{2n} since loop terms of length $2n$ are renormalized by "decorated loops" of longer lengths. These are paths that go along the loop with additional back-and-forth paths added to them. Such decorated loops have been discussed extensively, for

related problems, in Refs. 10 and 11, and can be summed up by use of simple combinatorics.

Equation (6.24) is the final result of this section and defines the quartic effective Hamiltonian $E^{\text{eff}}_{\text{quart}}$. Assuming we chose $\varepsilon=\varepsilon^*(S)$, the self-consistent value, then each term in $E^{\text{eff}}_{\text{quart}}$ is $\propto S\varepsilon^2$, i.e., $\propto(\ln S)^2/S$, in light of Eq. (5.2). We do not understand the discrepancy (by a factor of $1/S$) with logarithmic scaling of the fitted effective Hamiltonian in Fig. 8 and Eq. (5.7).

D. Discussion of loop derivation

With Eq. (6.24) we can completely understand the essential features of the quartic effective Hamiltonian, and how the analytic results of Sec. VI relate to the (prior) fit results of Sec. V. Equations (6.24) and (5.5) are both sums over the same kinds of loops. The terms do *not* have the same analytic functional form, but are related, in being minimized by the same configuration of alternating spins around that loop. Hence we understand how Eqs. (6.24) and (5.5) tend to be optimized by the same configurations, and hence why Eq. (5.5) was a good approximation of the correct effective Hamiltonian.

First, the leading-order term in Eq. (6.24) is due to hexagons. Since the number of AFM bonds within a single hexagon (in a π-flux state) can be 2, 4, or 6, and since $|U_{\mathcal{L}}|=2$ is the same for both the case of 2 AFM bonds and the case of 4 AFM bonds, then

$$\sum_{\hexagon} \varphi_{\mathcal{L}}|U_{\mathcal{L}}|^2 = -32\mathcal{P}_6 + \text{const}. \tag{6.25}$$

Thus, this term is in exact agreement the leading term in with Eq. (5.5). It accounts for the largest contribution, sufficiently large that our ground state search can be limited to the subset optimizing the hexagon term minimizing $|U_6|^2$ or equivalently maximizing $\mathcal{P}_6$.

The next to leading term is due to octagon loops. Already at this order, $|U_8|^2$ is *not* independent of $\mathcal{P}_8$. But, within π-flux states, an octagon has $\varphi_{\mathcal{L}}=+1$, and since $Q_8=-1$, then a large $|U_{\mathcal{L}}|$ is favored. Clearly, a large $\Sigma_{\octagon}|U_{\mathcal{L}}|^2$ means a tendency to alternate and this correlates with large $\mathcal{P}_8$, meaning that a large $\mathcal{P}_8$ is favored by Eq. (6.24). [In any case, among states optimizing Eq. (6.25), the octagon terms are always the same: see Appendix C 1.]

As for loops of length 10 or longer, the situation is further complicated because the pyrochlore lattice has more than one kind (modulo symmetries) of loops with this length, and $\varphi_{\mathcal{L}}$ may not be the same for different kinds of loop. Indeed, one kind of loop of length 10 has $\varphi_{\mathcal{L}}=+1$ while another kind has $\varphi_{\mathcal{L}}=-1$, in π-flux states. Therefore some loops of length 10 actually prefer to have a small $|U_{\mathcal{L}}|$, and it is not certain *a priori* that $\mathcal{P}_{10}$ should be maximized.

But the role of larger loops simplifies in the special case of the hexagon ground states (the subset of π-flux states that optimizes $\mathcal{P}_6$). The octagon terms [of either fitted effective Hamiltonian (5.5) or the analytic one, Eq. (6.24)] turn out to be the same for any of these states. Furthermore, at least for the stacked hexagon ground states found by the exhaustive search in Sec. V, and described in Sec. VI, many more terms are degenerate too. Each term appearing in Eq. (6.24) is the same in *every* state of this family, at least up to the terms for $|\mathcal{L}|=16$. Thus the degeneracy is broken only from a quite long loop that we anticipate to have a minuscule coefficient.

VII. DISCUSSION

We have calculated the anharmonic corrections to the spin-wave energy in the pyrochlore, and found that they break the degeneracy between the various harmonic ground states. We managed to numerically construct an effective Hamiltonian, and in Sec. VI, obtained an understanding of its terms.

In retrospect, we should not have been surprised to find that the effective Hamiltonian is written in terms of loop variables. After all, in any collinear configuration, the local environment that each spin sees is the same for all sites. If the centers of the tetrahedra were put on a Bethe lattice rather than a diamond lattice, then all collinear configurations would be related by lattice symmetries and would therefore have the same energy (as was found explicitly in the harmonic theory of Ref. 11 and the large-N theory of Ref. 10, and in analogy to Ref. 32). Thus any degeneracy-breaking terms *must* arise from lattice loops, so it is plausible that the effective Hamiltonian could be written explicitly in terms of loop configurations, but there are still multiple possibilities: the analytic derivation said that the loop term is the square of the number of antiferromagnetic bonds along it [Eq. (6.24)], whereas a good numerical fit was obtained to a Hamiltonian that counts only the loops with *all* bonds antiferromagnetic [Eq. (5.5)].

The anharmonic Hamiltonian is dominated by the smallest loops, the "hexagon" terms. The hexagon term's ground states are degenerate, having an $\mathcal{O}(L)$ entropy; we conjectured that the stacked family in Sec. V D are *all* of its ground states, but we did not demonstrate it (see Appendix C). Within those states at least (and certainly to octagon order in any hexagon-ground-state), the count of many longer loops is constrained so that only a tiny term can break the degeneracy, which (for the stacked family at least) is only at the length 26 loops. To the accuracy layers of our numerics, all the stacked ground states are degenerate.

What do our results say for realistic spins? First of all, the "small parameter" turned out to be $1/\ln S$, which is not really small except at unphysical spin lengths [$S=10$–10^3 were used for numerical fits in Sec. V C]. Still, our argument that only loop terms can break degeneracies still applies, so we expect the effective Hamiltonian takes similar functional forms for realistic S. It appears that only the first (hexagon) loop term will be important since this will fix the values of the next few terms and only some very long loops will cause quite small splittings in these energies. So in practice this leaves a massive but nonextensive degeneracy $\exp[O(L)]$, as was already the case for the harmonic ground state[11] (but with a smaller coefficient of L).

It is worth noting that the anharmonic selection effects in the pyrochlore turn out to be much weaker than in other closely related lattices: the two-dimensional checkerboard and kagomé lattices. In the checkerboard lattice, which we

discussed in Sec. IV, many of the details are the same as in the pyrochlore: it is composed of corner sharing tetrahedra, the spin-wave Hamiltonian is the same, and the harmonic ground states are collinear states with uniform fluxes. Nevertheless, because of the anisotropy inherent to the two-dimensional checkerboard, the anharmonic energy breaks the harmonic degeneracy at the lowest-order terms, of order $(\ln S)^2$.

In the kagomé lattice, the anharmonic selection is even stronger: first, there are cubic (in spin $\sigma^{x/y}$) anharmonic spin-wave terms. In addition, because of the anisotropy between in-plane and out-of-plane fluctuations about the coplanar states, *all* harmonic zero modes possess divergent fluctuations and therefore the anharmonic energy scales as a power law in S.[16–18]

Finally, we would like to mention that a similar calculation can be carried out in the case of collinear states with nonzero magnetization, in the presence of a magnetic field. Such magnetization plateaus have been the subject of numerous recent studies.[30,33–36] Our own harmonic work on the subject concluded that for a magnetic field that induces a collinear spin arrangement such that $\Sigma\eta_i=2$ in each tetrahedron, the degenerate harmonic ground states are zero-flux states.[11] One could develop a self-consistent variational treatment analogous to the one in this paper, to find that quartic ground state. Due to the asymmetry between ↑ spins and ↓ spins, there will be two independent variational parameters. In particular, the bond variables Γ_{ij} are no longer expected to satisfy Eq. (3.9). Rather, we expect the dominant terms in Γ_{ij} to be $\Gamma^0+(\eta_i-\eta_j)\Gamma^{(1)}+\eta_i\eta_j\Gamma^{(2)}$ (see Appendix A).

ACKNOWLEDGMENTS

This work was supported by the NSF under Grant No. DMR-0552461. We acknowledge the Cornell Center for Materials Research for use of its computer resources.

APPENDIX A: ORDINARY MODES

To attempt to understand the results of the anharmonic calculation, the first thing we try is to calculate the contribution to the anharmonic energy due to ordinary modes, as we did, for the checkerboard lattice, in Sec. IV B. The reason that we focus on ordinary modes is that, unlike generic zero modes, we know how they transform under gaugelike transformation. In the checkerboard case, we saw (Sec. IV B) that the anharmonic selection can be explained in terms of the correlations due to ordinary modes in the harmonic Hamiltonian. As we shall see below, this is not true for the pyrochlore lattice, i.e., the ordinary modes produce a gauge-invariant quartic energy.

1. Calculating correlations

An ordinary mode $\mathbf{v}_m$ is a mode that can be expressed in terms of a diamond-lattice mode $\mathbf{u}_m$ by Eq. (2.14). The correlation function G_{ij} was shown in Sec. II B 1 to be written as a sum over the spin-wave modes

$$G_{ij}=\sum_m \frac{S}{2|\mathbf{v}_m^\dagger \boldsymbol{\eta}\mathbf{v}_m|}v_m(i)v_m(j). \tag{A1}$$

Restricting ourselves to the contribution of ordinary modes (denoted henceforth by superscript "*ord*"), and using Eqs. (2.13) and (2.16),

$$G_{ij}^{\mathrm{ord}}=\sum_m{}^{\mathrm{ord}}\frac{S}{2|\lambda_m|}\eta_i\eta_j\sum_{\alpha,\beta:i\in\alpha,j\in\beta}u_m(\alpha)u_m(\beta),$$

$$=\eta_i\eta_j\sum_{\alpha,\beta:\in\alpha,j\in\beta}g_{\alpha\beta}. \tag{A2}$$

For Eq. (A2) we defined, in analogy with Eq. (A1)

$$g_{\alpha\beta}\equiv\sum_m{}^{\mathrm{ord}}\frac{S}{2|\lambda_m|}u_m(\alpha)u_m(\beta). \tag{A3}$$

We need bond variables (3.3), for a nearest-neighbor pair (ij), since that is how correlations enter our results [such as Eq. (3.8)]. To express this for a particular pair, let α be the common diamond site, and let β and β' be the diamond sites at the far ends of the bonds on which sites i and j sit, respectively. Then

$$\Gamma_{ij}^{\mathrm{ord}}=g_{\beta\beta}+g_{\beta\alpha}-g_{\beta'\alpha}-g_{\beta\beta'}. \tag{A4}$$

Note that the last line consists of one on-(diamond)-site correlation function, (the difference of) two nearest-neighbor correlations, and one second-neighbor diamond mode correlation.

2. Using the gaugelike symmetry

Although we have been considering one particular classical configuration, we can make use of the concept of gaugelike transformations (discussed in Sec. II B 2). The important points are the following:

(i) Under a gaugelike transformation $\boldsymbol{\tau}$ (recall $\tau_\alpha=\pm1$) the diamond-lattice spin-wave modes transform $u_m(\alpha)\rightarrow\tau_\alpha u_m(\alpha)$; $\eta_{i(\alpha\beta)}\rightarrow\tau_\alpha\tau_\beta\eta_{i(\alpha\beta)}$.

(ii) If two states have the same products of $\{\eta_i\}$ (flux) around each loop in the lattice, they are related by a gaugelike transformation.

(iii) In particular, if the state has a uniform flux arrangement, (e.g., the π-flux states), then *any* new configuration generated by a lattice-symmetry operation can alternatively be generated by a gaugelike transformation.

The consequences of these points is that, for the π-flux states,

$$\Gamma^{(0)}\equiv g_{\alpha\alpha}\quad\text{is independent of }\alpha \tag{A5}$$

(since a gaugelike transformation would take α to β for any two diamond sites α and β). Similarly, it is easy to find that for nearest-neighbor (diamond) sites α,β (sharing site i),

$$\Gamma^{(1)}\equiv\eta_i g_{\alpha\beta},\quad\text{independent of }i, \tag{A6}$$

and for next-nearest-neighbor (diamond) sites β,β', connected by bond (ij),

$$\Gamma^{(2)} \equiv -\eta_i \eta_j g_{\beta\beta'}, \quad \text{independent of } (ij). \tag{A7}$$

In Eq. (A7), the sign was set so that $\Gamma^{(2)}$ would be positive. Plugging these into Eq. (A4), we obtain

$$\Gamma_{ij}^{\text{ord}} = \Gamma^{(0)} + (\eta_i - \eta_j)\Gamma^{(1)} + \eta_i \eta_j \Gamma^{(2)}. \tag{A8}$$

Since Γ_{ij}^{ord} must be invariant under a global spin flip, we must have $\Gamma^{(1)} \equiv 0$ and we obtain

$$\Gamma_{ij}^{\text{ord}} = \Gamma^{(0)} + \eta_i \eta_j \Gamma^{(2)}. \tag{A9}$$

Equation (A9) is the key result of this appendix, the justification of Eq. (3.9). It should be noted that $\Gamma^{(0)}$ and $\Gamma^{(2)}$ are both infinite in the bare harmonic theory, and are regularized by the variational scheme. Here we assume that the regularization would not change the fact that $\Gamma^{(0)}$ and $\Gamma^{(2)}$ are spatially invariant and gauge independent.

Furthermore, by the argument above, $\Gamma^{(0)}$ and $\Gamma^{(2)}$ are the same for any harmonic ground state (π-flux state). Inserting Eq. (A9) into the mean-field energy (3.5), we quickly find that the ordinary-mode contribution to the anharmonic energy is gauge invariant,

$$\begin{aligned} E_{\text{MF}}^{\text{ord}} &= -\sum_{\langle ij \rangle} \eta_i \eta_j \left(\Gamma_{ij} + \Gamma_{ji} - \frac{1}{S^2} \Gamma_{ij} \Gamma_{ji} \right), \\ &= -\sum_{\langle ij \rangle} \left[\left(2\Gamma^{(0)} - \frac{(\Gamma^{(0)})^2 + (\Gamma^{(2)})^2}{S^2} \right) \eta_i \eta_j \right. \\ &\quad \left. + 2\left(\Gamma^{(2)} - \frac{(\Gamma^{(0)}\Gamma^{(2)})}{S^2} \right) \right], \\ &= N_s \left[2(\Gamma^{(0)} - 3\Gamma^{(2)}) - \frac{(\Gamma^{(0)})^2 + (\Gamma^{(2)})^2 - 6\Gamma^{(0)}\Gamma^{(2)}}{S^2} \right]. \end{aligned} \tag{A10}$$

Note that the arguments above do not apply to the checkerboard lattice, where all bonds are *not* equivalent by gauge transformations—there is no transformation that can take a diagonal bond and turn it into a horizontal or vertical bond. Therefore, the correlations calculated from ordinary modes are sufficient to break the harmonic-order degeneracy in that case, as we find in Sec. IV.

3. Relation of $\Gamma^{(0)}$ to $\Gamma^{(2)}$

We take a moment to note that the parameters $\Gamma^{(0)}$ and $\Gamma^{(2)}$ are not independent. We start from the variational Hamiltonian (Sec. III B). Notice that $\langle \mathcal{H}_{\text{var}} \rangle = E_{\text{harm}} + \mathcal{O}(\varepsilon)$. On the one hand, $\langle \mathcal{H}_{\text{var}} \rangle = E_{\text{harm}} + \mathcal{O}(\varepsilon)$ since [look at Eq. (3.14)] we could always do this well by using the wave function of the bare harmonic $\mathcal{H}_{\text{harm}}$. On the other hand, Eq. (3.4) [which is part of expectation (3.5)] contains terms in $\{\Gamma_{ij}\}$ which are divergent as $\varepsilon \to 0$: these must cancel out, at the dominant order. In other words, $\Gamma_{ij} + \Gamma_{ji}$, must cancel out,

$$\begin{aligned} \langle \mathcal{H}_{\text{var}} \rangle_{\text{dominant}} &= \sum_{\langle ij \rangle} \eta_i \eta_j (\Gamma_{ij} + \Gamma_{ji}) \\ &\approx N_{\text{FM}}[\Gamma^{(0)} + \Gamma^{(2)}] + N_{\text{AFM}}[\Gamma^{(0)} - \Gamma^{(2)}] = \mathcal{O}(\varepsilon). \end{aligned} \tag{A11}$$

Since Eq. (3.9) says Γ_{ij} (at dominant order) just depends on the sign of $\eta_i \eta_j$, the sum groups into N_{FM} terms for the FM bonds and N_{AFM} terms for the AFM bonds. But since $N_{\text{AFM}} = 2N_{\text{FM}}$ in any ground state,

$$\Gamma^{(2)}(\varepsilon)/\Gamma^{(0)}(\varepsilon) \to \frac{1}{3}, \tag{A12}$$

valid for the limit $\varepsilon \to 0$. Numerically, $\Gamma^{(2)}$ appeared to be between $\Gamma^{(0)}/3$ and $\Gamma^{(0)}/2$.

4. Role of generic zero modes

Note that in the entire discussion, we have ignored the generic zero modes. Recall that divergent modes occur along lines in the Brillouin zone at $\mathbf{q}$ values for which the ordinary-mode frequency goes to zero. For $\mathbf{q}$ values close to these divergence lines, the zero modes and small-frequency ordinary modes become close to each other (until they merge on the divergence lines; divergent modes are both ordinary and zero modes). The nearly divergent generic zero-mode contribution to the correlations mirrors the contribution of the nearly divergent ordinary modes, and therefore $\Gamma_{ij} \approx 2\Gamma_{ij}^{\text{ord}}$ and it has the same functional form, Eq. (A9).

In the self-consistent variational theory, the generic zero modes and the ordinary modes in the vicinity of the divergent lines interact strongly and, in fact, this interaction is responsible for the degeneracy breaking, as we observe in Sec. VI.

APPENDIX B: STACKED GROUND STATES

In this appendix, we analyze analytically the ground states of the effective Hamiltonians found in Secs. V C and VI C, as summarized in Sec. V D. We assume a stacked spin configuration (see Fig. 10) as this is what emerged from numerics; however, this is not yet proven.

1. Layer stackings

The pyrochlore sites can be broken into a stack of layers, each $a/4$ thick, where a is the lattice constant of the conventional cubic cell. The hexagon ground states are stackings of two kinds of slabs parallel to (say) the (001) plane: thin "A" slabs (thickness $a/4$) and thick "B" slabs (thickness $a/2$), which are stacked alternating A and B. A thin slab has one level of chains along the [110] or $[\bar{1}10]$ direction, along which the spins repeat the pattern "$+ \; - \; + \; -$." This pattern is reversed under a shift of $[a00]$ or $[0a0]$ so the periodicity is $\sqrt{2}a \times \sqrt{2}a$ within a thin slab.

A thick slab has two layers of spins, which form chains along the [110] and $[1\bar{1}0]$ directions, repeating the pattern "$+ \; + \; - \; -$," such that the chain spins are parallel and the

TABLE I. Types of spin patterns in π-flux hexagon loops. Only hexagons with a loop product $\varphi_{\mathcal{L}}=-1$ are included. Values are given for the two effective Hamiltonians, Eq. (5.5) and (6.24), from the next section.

Type	Class	Pattern	$-\mathcal{P}_6$	$\lvert U_6\rvert^2$
H_2	1	$(+\ +\ +\ -\ -\ -)$	0	4
H_2'	1	$(+\ +\ +\ +\ +\ -)$	0	4
H_4	2	$(+\ +\ -\ -\ +\ -)$	0	4
H_6	2	$(+\ -\ +\ -\ +\ -)$	−1	36

interlevel bonds are AFM in every tetrahedron spanning those two layers; within the thick slab, the spin pattern has a period $2a\times 2a$.

The interslab spin couplings cancel so each slab has an independent choice of two ways to align its spins. When there are m slabs of either kind, for a linear dimension in the stacking direction $L_z=m(3/4)a$, the number of stacked spin states is thus $3\times 2^{2m}=3\times 2^{8L_z/3}$. This includes three possible offsets (by multiples of $a/4$) in the z direction for the start of the stacking. [In a rectangular cell where L_x or L_y are also multiples of $3a$ (see below), we add similar terms counting possible spin stackings in the x or y directions.] Notice, apart that initial offset, the actual sites forming the layers are determined; only the spin directions are free.

As a side remark, we can compare this to the family of harmonic ground states for the pyrochlore as described in Ref. 9: that was a stacking of only A slabs. The family of ground states of the effective Hamiltonian derived in the large-N theory for the pyrochlore[10] is a stacking of alternating thin A' and B layers. The A' slab differs from the A layer shown in Fig. 10(a) in that the spin pattern is the *same* under a shift of $[a00]$.[37]

Now we examine the slab stacking more carefully. The way a B layer adjoins A layers on opposite sides forces successive A layers to have opposite orientations: i.e., if one slab has chains along $[110]$ the next one has them along $[1\bar{1}0]$, etc. On the other hand, the way an A layer adjoins its neighboring B layers requires these B layers to have a relative shift in the xy plane of $(a/4)[110]$ or $(a/4)[1\bar{1}0]$ parallel to the A layer's chains. Hence, the xy offset of the B layer cycles through all four possible values in successive B slabs. The result is any periodic stack must have m even, e.g., $m=2$ has a period $[a/2,a/2,3a/2]$ producing centered tetragonal cell. To directly repeat the same layer requires m to be a multiple of four so the shortest cell ($m=4$, $L_z=3a$) contains 12 layers of sites.

2. Counting short loops

Identifying ground states depends on counting the number of loops with various spin patterns, since this is what the effective Hamiltonian depends on. We first do it for the shortest loops, starting with hexagons. A hexagon that satisfies the π-flux constraint must have one of the four spin patterns shown in Table I); we label the types "H_{2m}," where $2m$ is the number of AFM bonds in the loop. Also, independent of the spin pattern, the sites of a hexagon are placed in two possible ways within the layer stacking, which are the "classes" explained in the next paragraphs; the classes are also labeled in Fig. 10.

First, there are two classes of hexagon placement. Class (1) hexagons are centered on thin slabs. The two spins in the thin layer are opposite, and each pair within a thick layer is parallel. Consequently, for each thin slab, the class 1 loops are half type H_2 and half H_2' (see Table I). Class (2) hexagons span one thick and one thin slab. The part of the loop within the thick slab always has $+\ -\ +\ -$, so for each thick slab, the class 2 loops are half type H_4 and half type H_6, of which the last is the type favored by the effective Hamiltonian. These are the four hexagon patterns satisfying the π-flux condition (1.4); that confirms that these slab stacked states are indeed harmonic ground states, a precondition for being hexagon ground states. Furthermore, since there are twice as many Class 2 hexagons as Class 1, exactly 1/3 of all hexagons are type H2 (the favored kind). Appendix F of Ref. 20 shows that a fraction 1/3 is the upper limit, so these are in fact hexagon ground states, too. A similar enumeration can be done of octagons. Again, for each particular type of spin pattern for an octagon, the number is the same for all our stacked hexagon ground states, therefore they are *degenerate* up to order eight.

3. Long loops

Symmetry can be used to show that much longer loops have the same count in all possible stackings. Say that a certain loop spans t slabs; the 2^t possible spin states of those slabs are defined by $(s_1,s_2,\ldots,s_t)$, where each $s_i=\pm 1$ is a reference spin in slab i. Now, a lattice-symmetry operation g (which maps each layer to itself) has the action effect of flipping the spins in some slabs and not others: i.e., $(s_1,s_2,\ldots,s_t)$ is multiplied by some pattern of $(\gamma_1,\gamma_2,\ldots,\gamma_t)$ of ± 1 factors, depending on g. Provided t is not too large, in fact *every* possible pattern of γ_i is generated by some one of the lattice symmetries: hence, all stacks of t slabs are related by symmetry and have the same counts of all possible loops. The smallest stack for which this no longer happens is when the first and last slab are stacked directly on top of each other, which (as worked out above) first happens for $m=4$, meaning 12 layers or for $t=9$ slabs (including the repeated one). The smallest loop which requires all of these slabs has length $2(12)+2=26$.

We conjecture that at order 26, the effective Hamiltonian *does* break the degeneracy. That will be a tiny energy: from Eq. (5.6) one could guess $\lvert C_{26}\rvert$ (for $S=100$) is in the range 10^{-7} to $O(10^{-3})$ (depending whether one assumes an exponential decrease with $2n$, or a power law).

APPENDIX C: GROUND STATE PROBLEM AS COLORING

Here we consider the ground states of the anharmonic effective hexagon-order Hamiltonian, $\mathcal{P}_6$. We review the arguments from Appendix F of Ref. 20. The key idea is that, in a π-flux state, there are constraints on spin arrangements due

TABLE II. Supertetrahedra types: frequencies in hexagon ground states, and the counts of hexagons in each supertetrahedron (using the type labels of Table I) The types are given color names as explained in text.

			Hexagons		
			H_2, H_2'	H_4	$H6$
Type	Name	Frequency	Orange	White	Purple
a	Purple	1/3	0	2	2
b		0	0	3	1
c	Orange	2/3	2	1	1
d		0	2	2	0

to the fact that different hexagons share edges. The level at which these constraints are first important is the *supertetrahedron*, a cluster in the form of a truncated tetrahedron with four hexagonal faces. The centers of the supertetrahedra form the *complementary* diamond lattice with the same lattice constant as the diamond lattice formed by centers of the original tetrahedron lattice. Each bond of the complementary diamond lattice (henceforth "superbonds") corresponds 1-to-1 with a hexagon in the original pyrochlore lattice.

We can classify supertetrahedra according to the types of hexagon loops appearing on their faces. Counting arguments there showed that there are four classes (Table II) and the total number of type 6 hexagons is maximized when only classes (a) and (c) appear.

1. Octagons in supertetrahedra

First we can apply the supertetrahedron enumeration to show that all the hexagon ground states also are degenerate at the octagon term; we take advantage of the fact that every octagon is contained entirely within one supertetrahedron (three contained in each).

We know that any hexagon ground state has fixed fractions of type (a) and type (b) supertetrahedra, as shown in Table II. But each of those supertetrahedra has a fixed pattern for its octagon loops: type (a) has one each of $(+\ -\ +\ -\ +\ -\ +\ -)$, $(+\ +\ -\ +\ -\ -\ +\ -)$, and $(+\ +\ -\ -\ +\ -\ +\ -)$, while type (b) has one each of $(+\ +\ -\ -\ +\ -\ +\ -)$, $(+\ +\ +\ -\ -\ -\ +\ -)$, and $(+\ +\ +\ +\ +\ -\ +\ -)$. Hence, any hexagon ground state has a fixed frequency of each octagon loop; from the list just given and the supertetrahedron frequencies in Table II, the octagon terms have the values $\mathcal{P}_8=1/9$, or mean $|U_8|^2=64/3$.

2. Node and superbond constraints as coloring rules

A convenient necessary (though not sufficient) condition to be a hexagon ground state can be expressed as the following coloring problem on the complementary diamond lattice. For this purpose, the hexagon types (which are the superbonds on this lattice) are associated with colors, as are the supertetrahedron types (nodes on the lattice). Then we have a complete covering by "purple trimers," consisting of two purple bonds (the middle node is purple and the other two nodes are orange. Simultaneously, we have a loop covering by orange loops (connecting orange nodes). Notice that, if we have such a coloring, we still must verify whether they can be filled in around each hexagon in a consistent fashion.

In the stacking of Sec. V D, the supertetrahedra centered in B slabs are of type (a), and those centered between A and B slabs are of type (c). The purple trimer bonds are all oriented vertically (i.e., the three nodes are always at three different levels); this give 2^2 degrees of freedom per B slab, accounting for all the spin entropy. The orange loops always run horizontally between the A and B slabs (perpendicular to the chains of that A slab).

We conjectured, but did not prove, that the *only* hexagon ground states were the stackings of Sec. V D. The special constraints of the stackings can be expressed, in the color language, as follows:

If α, β, γ, and δ are four successive nodes connected by orange bonds, then the $(\alpha\beta)$ and $(\gamma\delta)$ are oriented the same.

If β is orange and γ is a purple node, and $(\alpha\beta)$ is the white bond into β while $(\gamma\delta)$ is the purple bond out of γ, then $(\alpha\beta)$ is never oriented the same as $(\gamma\delta)$. We do not know if (i) and (ii) follow from the condition of having only type (a) and (b) supertetrahedra, and so we do not know whether any hexagon ground state exists, besides the stacked family of Sec. V D.

*Present address: Samsung Semiconductor Israel Research and Design Center, 10 Ohaliav St. Ramat Gan, 52522, Israel
†clh@ccmr.cornell.edu

[1] R. Moessner and A. P. Ramirez, Phys. Today **59**(2), 24 (2006).
[2] *Frustrated spin Systems*, edited by H. T. Diep (World Scientific, Singapore, 2005).
[3] Y. Motome and H. Tsunetsugu, Prog. Theor. Phys. Suppl. **160**, 203 (2005).
[4] O. Tchernyshyov, Phys. Rev. Lett. **93**, 157206 (2004).
[5] V. N. Kotov, M. E. Zhitomirsky, M. Elhajal, and F. Mila, Phys. Rev. B **70**, 214401 (2004).
[6] J. Villain, R. Bidaux, J. P. Carton, and R. Conte, J. Phys. (Paris) **41**, 1263 (1980).
[7] C. L. Henley, Phys. Rev. Lett. **62**, 2056 (1989).
[8] R. Moessner and J. T. Chalker, Phys. Rev. B **58**, 12049 (1998).
[9] C. L. Henley, Phys. Rev. Lett. **96**, 047201 (2006).
[10] U. Hizi, P. Sharma, and C. L. Henley, Phys. Rev. Lett. **95**, 167203 (2005).
[11] U. Hizi and C. L. Henley, Phys. Rev. B **73**, 054403 (2006).
[12] O. Tchernyshyov, H. Yao, and R. Moessner, Phys. Rev. B **69**, 212402 (2004).
[13] O. Tchernyshyov, O. A. Starykh, R. Moessner, and A. G. Abanov, Phys. Rev. B **68**, 144422 (2003).
[14] U. Hizi and C. L. Henley, J. Phys. Condens. Matter **19**, 145268

(2007).
[15] C. L. Henley, Can. J. Phys. **79**, 1307 (2001).
[16] A. Chubukov, Phys. Rev. Lett. **69**, 832 (1992).
[17] C. L. Henley and E. P. Chan, J. Magn. Magn. Mater. **140**, 1693 (1995).
[18] E. P. Chan, Ph.D. thesis, Cornell University (1994).
[19] Note that the choice of a *basis* within the subspace of generic zero modes *does* depend on the particular collinear state, as pseudo-orthogonality condition (2.10) depends on η.
[20] U. Hizi, Ph.D. thesis, Cornell University (2006).
[21] Γ_{ij} becomes symmetric in the large-S/small-ε limit we are interested in: see Eqs. (3.9) and (A9).
[22] A. B. Harris, C. Kallin, and A. J. Berlinsky, Phys. Rev. B **45**, 2899 (1992).
[23] M. Kvale (unpublished).
[24] To see this, set $q_x=\pi/2+\Delta q_x$, and the second term is $\eta_i\eta_j[(1/|\Delta q_x|-2|\Delta q_x|)\mathrm{sgn}(\cos q_y)-\sin q_y/|\cos q_y|]$, which, upon integration over q_y vanishes for arbitrarily small Δq_x.
[25] S. V. Isakov, K. Gregor, R. Moessner, and S. L. Sondhi, Phys. Rev. Lett. **93**, 167204 (2004).
[26] C. L. Henley, Phys. Rev. B **71**, 014424 (2005).
[27] In Ref. 13 the polarization axis of checkerboard tetrahedra was denoted by a color Potts variable.
[28] It should be noted, however, that when we impose a gaugelike transformation, e.g., along a horizontal line, we are forced to change the vertical boundary condition from periodic to antiperiodic or vice versa.
[29] J.-S. Bernier, C.-H. Chung, Y. B. Kim, and S. Sachdev, Phys. Rev. B **69**, 214427 (2004).
[30] D. L. Bergman, R. Shindou, G. A. Fiete, and L. Balents, Phys. Rev. Lett. **96**, 097207 (2006).
[31] D. L. Bergman, R. Shindou, G. A. Fiete, and L. Balents, Phys. Rev. B **75**, 094403 (2007).
[32] B. Douçot and P. Simon, J. Phys. A **31**, 5855 (1998).
[33] H. Ueda, H. A. Katori, H. Mitamura, T. Goto, and H. Takagi, Phys. Rev. Lett. **94**, 047202 (2005).
[34] K. Penc, N. Shannon, and H. Shiba, Phys. Rev. Lett. **93**, 197203 (2004).
[35] M. E. Zhitomirsky, A. Honecker, and O. A. Petrenko, Phys. Rev. Lett. **85**, 3269 (2000).
[36] S. R. Hassan and R. Moessner, Phys. Rev. B **73**, 094443 (2006).
[37] These states were illustrated in Fig. 3 of Ref. 10 with the stacking in the x direction, the B layers being those with all bonds AFM, or gray in that figure.